Analysis of Perisaccadic Field Potentials in the Occipitotemporal Pathway During Active Vision

Keith P. Purpura, Steven F. Kalik, and Nicholas D. Schiff
Department of Neurology and Neuroscience, Weill Medical College and Graduate School of Medical Sciences of Cornell University, New York, New York 10021

Purpura, Keith P., Steven F. Kalik, and Nicholas D. Schiff. Analysis of perisaccadic field potentials in the occipitotemporal pathway during active vision. *J Neurophysiol* 90: 3455–3478, 2003. First published July 23, 2003; 10.1152/jn.00011.2003. Eye movement potentials (EMPs) associated with saccades appear in both subcortical and cortical structures of the primate visual system. In this study, EMPs are recorded across sites in the occipitotemporal (OT) pathway of monkeys performing a pattern-recognition task. We characterize pair recordings of saccade-triggered local field potentials (LFPs) in early extrastriate and inferotemporal regions of the ventral visual pathway using time–frequency spectrograms. Parameters of the spectrograms, including the centroids of identified regions of interest in the time–frequency plane, are extracted and analyzed. Comparisons among the distributions of the extracted parameters reveal that the occipital lobe EMPs are largely postsaccadic events centered at 100 ms after saccade onset that are typically not influenced in timing by the direction of the saccade or the appearance of a stimulus transient appearing either before or after the saccade. The occipital lobe EMPs also demonstrate a significant shift in frequency content during their transient time course that is influenced, in a few cases, by saccade direction. Temporal lobe EMPs, on the other hand, may be centered in either the presaccadic or postsaccadic intervals; the time of their appearance is significantly influenced by the direction of the saccade. Temporal lobe EMPs demonstrate less frequency modulation than those recorded in the occipital lobe. The prevalence of EMPs in the OT pathway suggests that many cortical regions important for pattern recognition can be modulated by saccades. The timing and frequency characteristics of these signals suggest that the nature of this perisaccadic modulation varies across the cortex.

INTRODUCTION

Saccadic eye movements generate a brief field potential that can be recorded from many locations in the brain. In human subjects, a class of transient voltage waveforms closely timed to the execution of saccades (lambda waves) can be recorded from occipital and parietal EEG leads during periods of wakefulness (Evans 1953; Green 1957). These signals appear at the end of the saccade and are differentially modulated by the direction of the eye movement (Skrandies and Laschke 1997). Tasks requiring attention, such as reading, increase the amplitude of these signals and shorten their latency (Barlow 1971; Fourment et al. 1976).

In animals, saccades are correlated with transient local field potentials (LFPs) in the lateral geniculate nucleus (LGN) of the monkey and cat (Brooks and Gershon 1971; Feldman and Cohen 1968; Jeannerod and Sakai 1970), and in the temporal (Sobotka et al. 2002), parietal (Pesaran et al. 2002), and frontal lobes (Klostermann et al. 1994; Seidemann et al. 2002) of the cerebral cortex and mesolimbic structures (septum and hippocampal formation: Sobotka and Ringo 1997) of the monkey. As with the human scalp-EMPs, the LFP-EMPs recorded in mesolimbic structures of the alert monkey are differentially modulated by the direction of the saccade and by the visual environment (Sobotka and Ringo 1997). In a lighted environment, these LFP-EMPs are generally faster (shorter latency for time-to-peak) and more biphasic (larger peak-to-trough excursions) than in the dark.

A strong extraretinal contribution to the EMPs is emphasized by the following observations: *1)* complete retinal loss through optic nerve section or photocoagulation does not entirely eliminate EMPs in the cat LGN (Brooks and Gershon 1971; Jeannerod and Saki 1970); *2)* EMPs in the cat cortex and LGN appear both with caloric stimulation of the labyrinths under flaxedil paralysis sufficient to prevent saccades and with electrical stimulation of the pontine reticular formation with concomitant saccades when the paralytic is removed (Brooks and Gershon 1971); *3)* EMPs are not produced in the monkey LGN by rapid mechanical displacement of the eye (Feldman and Cohen 1968).

Taken together, both the human and animal studies suggest that EMPs represent a signal in thalamic and cortical populations that is produced, in part, by the networks responsible for generating and controlling saccadic eye movements. The appearance of EMPs in the LGN, ventral visual pathway (including the temporal lobe), and mesolimbic structures—all regions of the brain not typically included in the oculomotor network (Wurtz 1996)—may therefore reflect the arrival of corollary motor activity (McCloskey 1981; Sommer and Wurtz 2002). Such corollary discharge signals may originate in the brain stem, superior colliculus (SC), lateral intraparietal area (LIP), and/or the frontal eye fields (FEF). The role of this corollary activity in the occipitotemporal (OT) pathway has not been fully resolved.

Here we examine EMPs in alert monkeys performing a pattern-recognition task. The timing and frequency content of

---

EMPs, their regional differences in the OT pathway, their interactions with visual transients, and the influence of behavior (direction of saccadic eye movement) on their dynamics are quantified. Our goal is to determine, in more detail, the extent to which EMPs reflect corollary motor signals, to suggest how they are generated, and what their role may be in active vision.

The relationship between EMP signals recorded in the OT pathway and corollary oculomotor activity can be clarified by the temporal relationship between the time of saccade onset and the change in power in local population activity. For example, activity that precedes and is coincident with saccade onset may be associated with remapping of receptive fields (Duhamel et al. 1992; Umeno and Goldberg 1997; reviewed in Ross et al. 2001), "interrupts" from attentional circuit breakers (Corbetta and Shulman 2002) that lead to the generation of orienting saccades, and executive commands originating in the frontal eye fields that are associated with the selection of targets and implementation of scan paths (Bruce et al. 1985). Because of their timing, these EMPs cannot be generated by the visual reafference, the activity generated in the retina by the movement of the eye. On the other hand, activity that follows saccade onset and offset may represent either visual reafference or the exafference activity, that is, the activity produced by an interaction between the visual reafference and the corollary discharge (McCloskey 1981).

In addition to the timing of these signals with respect to saccade onset, other characteristics may also be useful for illuminating the origin of EMPs and their relationship to active vision. For example, regional differences in the timing and frequency content of EMPs would suggest that signals related to saccadic eye movements enter and influence the different stages of visual processing in the OT pathway through a variety of channels. Directional EMPs would indicate that the oculomotor network provides a significant component to the saccade-related activity in the OT pathway. Finally, interactions between visual transients and EMPs can be evaluated in terms of the gating of visually evoked activity by the saccade and its corollary activity.

We recorded LFPs using high-impedance microelectrodes at locations in the occipital and temporal lobes of monkeys during a task that required sustained attention and the scanning of a series of high-contrast dynamic images, conditions that maximize the amplitude and shorten the latency of EMPs (lambda waves). We examine the LFPs in a 500-ms interval centered on the onset of the horizontal component of saccades made during the trials. Here we seek to produce a time–frequency representation of the average LFP around the time of the saccade as one might do when processing acoustic signals that have a high signal-to-noise ratio. The EMP is not subtracted from each saccade-triggered LFP in the time-domain before spectral analysis. Instead, a spectrogram is computed for a number of different estimates of the EMP to establish confidence intervals for the EMP spectrogram. Time–frequency spectrograms are calculated to capture a portrait of the presaccadic, transsaccadic, and postsaccadic activation generated in the local cortical population. The spectrograms are evaluated to determine the influence of saccade direction, cortical location, and timing of visual transients on the time and frequency content of the LFPs during the perisaccadic interval.

METHODS

Physiology and behavior

LFPs were recorded from sites within the occipital and temporal lobes of 2 adult male macaque monkeys (*Macaca mulatta*), monkeys M and S, performing a pattern-recognition task. All animal care and both surgical and experimental procedures conformed to guidelines established by the National Institutes of Health and the Institutional Animal Care and Use Committee of the Weill Medical College of Cornell University.

RECORDING LOCATIONS. Using sterile surgical technique, recording chambers (Crist Instrument) and a head holder were attached under isoflurane general anesthesia to the skulls of the monkeys at positions selected to provide access to regions of the extrastriate visual cortex in both the occipital and temporal lobes. For monkey M, one chamber was placed over the occipital lobe (P12, L20) and a second chamber was centered over the temporal lobe (A10, L21). Both of these chambers were placed over the right hemisphere. For monkey S, 3 chambers were used: occipital lobe chambers for the left and right hemispheres (P12, L20) and a right hemisphere temporal lobe chamber (A10, L21). The recording chamber placements were made after MR imaging (T1-weighted images made in a 1.5-T field, juvenile head coil) with the animal held in an MR-compatible stereotaxic frame that was then used in the subsequent surgeries. With monkey S a second set of images was taken during the course of the studies with tungsten microelectrodes left at productive recording sites. A custom-designed head coil was used for this second imaging session and the axial, sagittal, and coronal images were combined into a full 3-dimensional volume to better trace the path of the microelectrodes through the brain. For monkey M, some of the elements used for building the cranial implant were made of steel, so it was not possible to obtain an MRI after surgery. Instead, a fluoroscope was used to produce images of the microelectrodes and guide tubes in vivo.

Based on the imaging data, and with reference to a recently published *Macaca fascicularis* atlas (Martin and Bowden 2000), detailed microelectrode track reconstructions relating depth to receptive field size and eccentricity (Gattass et al. 1988), and from our own single unit recordings, we assigned our occipital lobe LFP recording sites as follows: V1 for recording depths in the range of 0–1.6 mm; V2–V3, 2–8 mm; ventral V1–V2, 8–14 mm. Ventral V4 was at the same depth as ventral (upper and parafoveal visual field) V1–V2 but accessed from more anterior positions in the chamber. The temporal lobe recordings were subdivided into 3 groups. The first, shallower group of visual units and LFP responses encountered in the temporal lobe tracks (at depths of 18–20 mm in monkey M, and starting at 16 mm in monkey S) were assigned to the inferior bank of the superior temporal sulcus (STS). The deeper recordings, encountered after passing through a region devoid of single units (white matter), were assigned to the inferotemporal cortex (area TE at depths beginning at 29 mm in monkey M). More medial penetrations at this depth entered the parahippocampal gyrus (PHG).

LOCAL FIELD POTENTIAL RECORDING. Extracellular recordings were made with epoxy-insulated tungsten microelectrodes (FHC, Bowdonham, ME), with a nominal impedance of 1–4 MΩ. All the data reported here were obtained by recording simultaneously with 2 microelectrodes. In one series of recording sessions, one electrode was placed in the occipital lobe with the other electrode placed at temporal lobe sites (monkeys M and S). In the other series of experiments, one electrode was placed in the left occipital lobe and the second microelectrode was situated in the right occipital lobe (monkey S). The microelectrodes were advanced with hydraulic microdrives (Narashige) through guide tubes inserted through the dura. For the temporal lobe recordings the guide tubes were lowered 13 mm into the brain to protect the microelectrode tips and to straighten the trajectory of the microelectrode travel. A grid system (Crist Instrument) was used in the chambers to organize guide tube placements.

The signals from each electrode were separated into spike and LFP channels (Tucker-Davis Technologies, Gainesville, FL). After appropriate band-pass filtering the LFPs were sampled at 200 Hz and the 1- to 10-kHz channels were sorted on-line for spike shapes with either matched template filters or neural network classifiers (Chandra and Optican 1997).
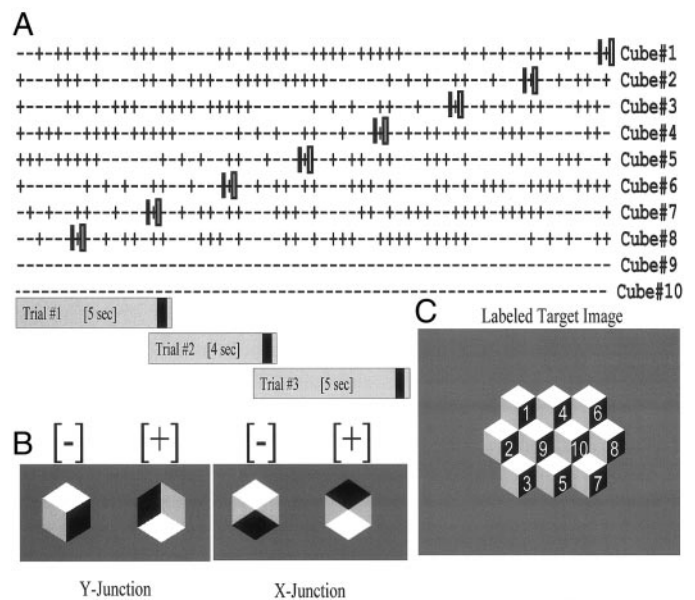
All the recordings were monopolar with the ground tied to either skull screws (monkey S) or a scalp EEG lead (monkey M). The same ground was used for both microelectrodes in the dual recordings. Monopolar LFP recordings (like those reported here) are not as localized as single-unit or bipolar LFP recordings, nor as delocalized as scalp EEGs and visually evoked potentials (VEPs). An important question is: how localized or delocalized are these LFP recordings? In a separate series of experiments we demonstrate that EMPs extracted from monopolar LFP recordings vary significantly across distances as little as 400 μm along vertically oriented electrode tracks. These data and the relevant methods of analysis are explored in SUPPLEMENT 3 (the Supplemental Material is available at the *Journal of Neurophysiology* web site).[1]

ASSESSMENT OF VISUAL ACTIVITY. All of the LFP recordings were obtained from positions in the recording track associated with single-unit and multiunit activity. Visually driven units were located by detecting the presence of modulated responses to a checkerboard pattern that could be varied in contrast, check size, check aspect ratio, and frequency of stimulation period (as appearance–disappearance or contrast–reversal). After isolation of single units, activating regions (Snodderly and Gur 1995) of some of the units were outlined by hand with a mouse controlling the positions of bars and squares, and the rate and type of contrast modulation (black–white, red–green). In many recording sessions, a standard checkerboard m-sequence (50 Hz), sized to cover one of the hand-mapped receptive fields, was run with the animal performing a concurrent fixation task.

EYE MOVEMENT RECORDING AND DETECTION OF SACCADES. The monkeys' heads were fixed to the primate chair through the implanted head holder during all of the recording sessions. Eye position measurements were recorded using the horizontal and vertical analog outputs from the E5000 infrared video eye-tracking system (ASL, Bedford, MA). The animal's gaze position was calibrated each day before experiments began, and then whenever necessary to ensure the accuracy of the calibration. Horizontal and vertical signals were processed to determine the occurrence of a saccade, its amplitude, velocity, direction, and positions of fixation.

Saccade onset is detected when the eye speed surpasses a threshold equal to the smallest reliable difference (about 1.3°) between 2 consecutive positions divided by 10 ms (2 × temporal sampling resolution of the eye tracker signals), corresponding to 130°/s. Saccade end is detected when the velocity falls back below the threshold. Saccades that are preceded by signals with unusually low variance, such as a flat line attributed to the loss of signal (as can be produced by a blink), are not included in the analysis. The average position recorded during periods that have signal but no detectable velocity components are taken as the centers of positions of fixation. Saccades that are separated by a fixation period ≤80 ms are fused through interpolation if they are both in the same cardinal direction (left, right, up, down) and discarded if they are not.

EXPERIMENTAL CONTROL AND BEHAVIORAL TASK. The monkeys performed a pattern-recognition task that required them to report the appearance of a target during the presentation of a sequence of similar images. The rate of image change (2, 3, or 4 Hz) was kept in a range that produced better than chance performance on the tasks. Shown in Fig. 1C is the target image with superimposed numerals indicating the temporal modulation sequence (Fig. 1A) assigned to each hexagonal region ("cube") in the image. The modulation moves the white dia-

FIG. 1. Organization and control of stimulus set used for pattern-recognition task. A sequence of images is produced by modulating the appearance of a number of subregions labeled 1–10 in *C* (numbers are presented here only to aid in description of stimulus). Modulation for each region is determined by a sequence of +'s and −'s shown for all subregions in *A*. For example, row labeled Cube#1 in *A* controls the appearance of hexagonal region 1 in *C*. The "−" state corresponds to placing the white diamond at top of each hexagonal subregion (for "Y" or "X" junctions in *B*) and "+" corresponds to having the white diamond at the bottom of the subregions. Configuration of subregions for target stimulus (pattern that must be recognized) is shown in *C*. Sequences are broken up into shorter segments for behavioral trials. Three such trial periods underline modulation sequences in *A*. The dark bar at the end of each trial period indicates when target is shown. Pairs of vertical bars in modulation sequences in *A* indicate where the m-sequence ends (filled vertical bar) and begins anew (open vertical bar). Note that for each subregion (Cubes #1–8) the modulation sequence is identical but shifted in time by a number of steps.

mond from the top (−1, Fig. 1*B*) to the bottom (+1, Fig. 1*B*) of the hexagonal region; for the "Y"-junction this produces what appears to be a cube viewed and lighted from above (−1) or a cube viewed and lighted from below (+1). Eight of the 10 regions are modulated, whereas the center 2 regions (9, 10) are static. The modulation sequence is a 6th-order m-sequence (63 elements in length) (Sutter 1992). The 8 modulated cube regions are assigned to different shifts of the m-sequence. In this study, the neural activity was not correlated against the m-sequence to produce estimates of the responses to the appearances of either of the elements (−1 or +1) in Fig. 1*B* at each of the eight positions (1–8) in Fig. 1*C* (this is reported in Purpura et al. 1999). Here the modulation sequence is used to produce a set of images whose subregions (cube elements) are nearly uncorrelated in space and in time when considered pairwise, and also have nearly zero higher-order correlations at each position for up to 6 transitions in the past. At least one cube element is modulated on each transition and, on average, 4 of the elements are flipped.

The use of an m-sequence to specify the transitions in the subregions and the relationship between the transitions in different subregions reduces the degree of correlation between subsequent samples of the stimulus. This will be true whether the visual system samples a sequence in the stimulus through extended periods of fixation or by selecting different regions of the stimulus by making attentional shifts and saccades across the display. Thus the saccade-related neural activity in the perisaccadic interval will be less influenced by correlations in the visual display. Presaccadic spatial adaptation has been shown to influence the responses to visual stimuli presented during a saccade (Judge et al. 1980) and after the saccade (Gawne and Woods 2003). Here we have balanced these potential effects by presenting the

same cube configuration (−1 or +1, followed by −1 or +1, respectively; see Fig. 1*B*) as often as the opposite configuration (−1 or +1 followed by +1 or −1, respectively) in subsequent frames in many regions of the stimulus. Having only one instance of pattern appearance at the beginning of each trial, followed by a period of pattern modulation, also provides a more balanced sequence of visual inputs across the trials: the overall values of luminance in each of the hexagonal subregions are the same for both configurations −1 or +1 (Fig. 1*B*), and regions of contrast modulation are fragmented in time and space across the sequence of images and trials.

Subsequences of the m-sequence were presented on each trial. The sequences overlapped on subsequent trials. A new trial always began one slot behind where it ended at the termination of the last trial, before the last presentation of the target. In Fig. 1*A* staggered bands (labeled "Trial #1," "Trial #2," and "Trial #3") beneath the m-sequences indicate which configurations of the multi-input m-sequence were used in each of the 3 trials shown. A vertical bar within each band shows where the target replaced the next configuration in the sequence. The length of each trial was selected at random from a choice of 0 (a catch trial where only the target is shown), 2, 4, 5, or 6 s before appearance of the target. In the examples shown here, the first 3 trials would run for 5, 4, and 5 s. Recognition of the target is signaled by a bar release between 150 to 600 ms following the target. The target is followed by the next configuration in the multi-input m-sequence to provide a backward mask of the target before the screen is returned to a featureless mean gray background. The size of the liquid reward (juice or water) is scaled to the length of the trial.

The visual stimuli were presented on a Mitsubishi XC-2930C CRT (27° H × 21° V screen) placed 114 cm in front of the monkey. Images were displayed with a frame rate of 95.5 Hz. The mean luminance of the featureless gray background was 50 cd/m² with the white, light gray, and dark gray regions of the hexagonal elements (Fig. 1*B*) at 100, 80, and 15 cd/m², respectively. Each hexagonal region, or cube, was approximately 3.5° H × 4° V, with the overall configuration of 10 conjoined cubes subtending about 14° H × 10° V on the screen (Fig. 1*C*). The surrounding gray background was left on the screen between trials. Graphics were produced with a VSG 2/3 (Cambridge Research, Cambridge, UK) video board running on a Pentium PC. Real-time control of the graphics computer, monitoring and recording of gaze position, recording of neural activity, monitoring behavioral responses, and reward delivery were performed with a second Pentium PC running TEMPO (Reflective Computing, St. Louis, MO). Coordination of the 2 PCs was administered through a proprietary data transfer protocol (Reflective Computing).

GROUPINGS OF SACCADES FOR ANALYSIS. Saccades are generated in a number of different contexts during the trials. In this study, we consider groupings based only on the presence of a significant horizontal component in the eye movement signals. We classify the saccades into different analysis groups based on several factors: *1*) The direction of the saccade with respect to the laterality of the recording site. Saccades are thus either contraversive (directed away from the hemisphere of the brain containing the recording site) or ipsiversive (directed toward the recording site). *2*) The direction of the saccade in body-centered coordinates; that is, leftward saccades are to the left side of the body. *3*) The time of a stimulus sequence interchange (visual transient) with respect to the time of the saccade in the 500-ms analysis window centered on the saccade. Groups are formed for: *i*) saccades that are preceded (within 250 ms) by a visual transient; *ii*) saccades that are followed (within 250 ms) by a visual transient; *iii*) saccades produced between 2 visual transients occurring within the same 500-ms window (3- and 4-Hz stimulation). *4*) Consecutive contraversive (or leftward) saccades are placed in 2 separate groups as are consecutive ipsiversive (rightward) saccades. This separation is made to reduce the confluence of the postsaccadic phase of one leftward saccade, for example, with the presaccadic phase of the next, or previous, leftward saccade. Consecutive saccades that have the

same direction but that are separated by <250 ms are dropped from the analysis.

All of the analysis groups for the EMPs were established before any statistical testing. The goal here was to first organize the field potential data by behavioral criteria such as the direction of saccade and then establish whether intrinsic components of the EMP waveforms could be segregated based on statistical tests.

Figure 2 illustrates how a sequence of saccades made over 2 trials is divided into analysis groups L1, L2, R1, and R2. Successive saccades in the same direction are alternately assigned to *groups 1* and *2* (L1 and L2 or R1 and R2) regardless of the presence of intervening saccades of the opposite direction. For example, beginning with the first leftward saccade in *Trial 1*, every other leftward saccade is assigned to *group L1* even if a rightward saccade intervenes or a new trial commences. The other leftward saccades are assigned to *group L2*. The rightward saccades are similarly assigned to *groups R1* and *R2*. In this example, by the end of *Trial 2*, there will have been 3 L1 saccades, 2 L2 saccades, and 3 each of R1 and R2.

Data analysis

SPECTROGRAMS. Among the features one would like to collect from saccade-triggered averages of LFPs are: *1*) the time-to-peak power in the signals; *2*) the shape of the waveforms [are they dominated by one sinusoidal component or do they exhibit frequency modulation (FM)?]; *3*) the extent to which they are influenced by the timing of stimulus transitions in the perisaccadic interval, saccade direction, and recording location.

Dominating this type of analysis, as with the analysis of all evoked field-potential data, are questions concerning what components of the LFP activity are robust and how much confidence can one place on the estimates of such extracted features. LFP averages are often about one-fourth to one-tenth the amplitude of the range exhibited on individual trials. Thus the issue becomes, in the face of a relatively low signal-to-noise ratio, what is the most efficient way of analyzing such data. The answer is to make estimates in a restricted range in the spectrotemporal domain (Percival and Walden 1993) using an approach that allows multiple independent estimates to be made from the same data set. Multitaper spectral analysis (Thomson 1982) provides a means to produce such estimates; the availability of these multiple estimates improves the reliability of conclusions that can be made about features extracted from the physiological signals of interest. Multitaper spectral analysis also establishes a rigorous set of guidelines for obtaining an optimal tiling of the spatiotemporal domain that avoids violating theoretical limits imposed on time and frequency by the uncertainty relation (Jarvis and Mitra 2001; Mitra and Pesaran 1999; Percival and Walden 1993).

The difficulty with spectral estimation is that the statistical properties of samples of neural activity change with time, violating the stationarity requirements of all spectral analysis methods. It is some-

	TRIAL 1						TRIAL 2			
	L	L	R	L	L	R	R	L	R	R
L1	x			x				x		
L2		x			x					
R1			x				x		x	
R2						x			x	x

FIG. 2. Example of saccade assignments to analysis groups. Illustration of how a sequence of saccades recorded over 2 behavior trials would be divided into different analysis groups. Over 2 trials, 3 leftward saccades would be assigned to L1, 2 leftward saccades would be assigned to L2, and 3 rightward saccades would be placed in both R1 and R2 analysis groups. During actual behavioral trials, visual transients (m-sequence transitions) are also occurring. Thus assignments to analysis groups are also made on the basis of whether a visual transient occurs in presaccadic or postsaccadic phase, or in both pre- and postsaccadic phases of the perisaccadic interval.

times possible to produce cyclo-stationarity by taking samples collected during repetitive stimulation or repeated behavioral actions. During the temporal intervals defined by these sampling procedures, however, the neural activity is often still nonstationary. To produce an estimate of how the spectrum of the LFP changes with time around the saccade we calculate Thomson's high-resolution multitaper spectrogram (Thomson 2002) using the saccade onset time to define the temporal interval for drawing samples from the trials. Spectrograms minimize the violation of the stationarity requirement by calculating spectral quantities over a smaller temporal window in the interval of interest, in our case the perisaccadic interval, and shifting the window over that interval. A brief description of Thomson's version of the spectrogram technique is provided in SUPPLEMENTS 1 and 2 (the Supplemental Material is available at the *Journal of Neurophysiology* web site).[2]

ESTIMATE OF THE STANDARD ERROR IN THE SPECTROGRAM.   The goal here is to extract features from the spectrograms of the average LFPs to characterize how saccades modulate the neural activity in local cortical populations. Spectrograms are 2-dimensional (2-D). As such, a salient feature or region within a spectrogram can be defined by its area, the orientation and eccentricity of a best-fitting ellipse, and the 2-D coordinates of its centroid. Thus one problem with carrying out such a region-of-interest (ROI) analysis is determining what is a salient and robust feature in the spectrogram. Here, we establish a threshold level of power spectral density in each spectrogram (see APPENDIX A). This value is then compared point by point in the spectrogram with a 95% confidence interval for the mean computed at each point using all the samples in a subset (e.g., those associated with rightward saccades only) of the LFPs. If a point in the spectrogram has a confidence interval that does not bracket the threshold (noise) level for the spectrogram, then this point is included in a region of interest. If the threshold value does fall within the point's confidence interval, then that point in the spectrogram is set to zero power spectral density.

Each LFP sample referenced to a saccade contributes additively and independently to our estimate of the spectrogram of the saccade-triggered average LFP. As a consequence, the jackknife standard error calculation can be used to produce a confidence interval for the spectrogram of the mean LFP (Efron and Tribshirani 1998; Thomson and Chave 1991). This is shown in APPENDIX A.

ROI (REGION-OF-INTEREST) ANALYSIS.   To extract statistically significant regions from the spectrograms we need to define the lower bound and the maximum value for the distribution of values in the spectrogram (S_{avg} in APPENDIX A). The estimates of the lower bound and maximum are used as inputs to the MATLAB function (MATLAB, v6.1) ROICOLOR. This function determines the coordinates in a 2-D array where the power ranges between 2 levels. We have chosen a noise level (see APPENDIX A) and an estimate of maximum power (see APPENDIX B) in the spectrogram as the 2 levels. The extracted regions are then passed through a continuity filter (BWLABEL function, MATLAB) to determine which of the values in the ROI are connected to other values in the spectrogram by more than the corners of a time–frequency pixel. The assumption here is that continuity in the time–frequency plane reflects waveform integrity in the LFPs. Because the spectrograms have been tested against a threshold (noise level) before application of ROICOLOR and BWLABEL, the ROIs are maps of areas in the spectrograms that have significant power as determined by the jackknife procedure.

Using the MATLAB function REGIONPPROPS, we also extract the values of several parameters from each ROI. These parameters include the area, the coordinates of the centroid (centers of mass), and the orientation and eccentricity of a best-fitting ellipse. The areas of the ROIs are used to identify the largest ROI in a spectrogram. The centroid of an ROI is its weighted center. The weights are formed

from the distributions of power in the frequency and time domains. This estimate uses all of the data describing a region, so focusing on the largest ROIs strengthens the estimate of its centroid.

RESULTS

We report here on the analysis of recordings made at 34 pairs of sites, arranged in either the occipital lobe–temporal lobe recording configuration (20 from monkey M, 6 from monkey S), or in the left occipital–right occipital lobe configuration (8 in monkey S only). During these recordings, a number of visual experiments were run including several variations of the pattern-recognition task described in METHODS including changes in m-sequence interchange rate (2, 3, or 4 Hz) and a substitution of X-junctions (see Fig. 1*B*) for Y-junctions in the hexagonal regions in the images that precede the appearance of the target. In the present study our goal is to characterize the EMPs generated during the execution of saccadic scan paths. Although there is some evidence for coupling between the organization of the saccade sequences and the temporal rate of interchange and the nature of the junctions (Kalik et al. 1999), we will treat these different types of runs as only repeats of the same pattern-recognition task for the analyses presented here.

Studying active vision

An illustration of the events constituting a typical trial is shown in Fig. 3. Once the monkey's gaze enters the screen and dwells there for ≥250 ms, the first configuration slotted for the current trial appears (Fig. 3*A*, *image frame 49*). In this trial, 10 configurations are presented (interchange rate of 2 Hz) before the target is displayed (Fig. 3*B*, *top row*, *image frame 127*). As can be seen from the eye movement traces in Fig. 3, the monkey was free to shift its gaze within a region bounded by the screen during the course of the trial. Eight saccades with detectable rightward components and 10 saccades with leftward components can be extracted from the eye movement records for this trial. The eye movement traces and LFPs recorded simultaneously in the occipital and temporal lobes for this trial are shown in Fig. 4. A typical recording session provided behavioral and neural data from 250 similarly organized trials.

As seen in Fig. 4, LFPs recorded in both occipital (V2) and temporal lobe (TE) sites contain contributions from external visual transients, and an additional set of transients more closely correlated with the times of saccades (asterisks in V2 LFP). Our goal here is to characterize the spectrotemporal content of the neural activity in an interval surrounding the saccades so that the activation time of the EMP can be reliably determined and associated with a particular saccade and recording location. The emphasis here is on the average LFP activity triggered by the saccade (the EMP). The average LFPs obtained from all the trials in one recording session, using saccade onset time for the averaging reference, are shown in Fig. 5, *A* and *B*. Transient components in the V2 and TE LFPs are seen in the perisaccadic intervals centered on the saccades. The saccades with significant leftward (contraversive) and rightward (ipsiversive) horizontal components are associated with different average LFP waveforms. For the V2 and TE recordings, the rightward saccades produce larger transient average LFPs in the postsaccadic interval. We will see later

---

[2] The Supplemental Material for this article is available online at http:// jn.physiology.org/cgi/full/00011.2003/DC1.
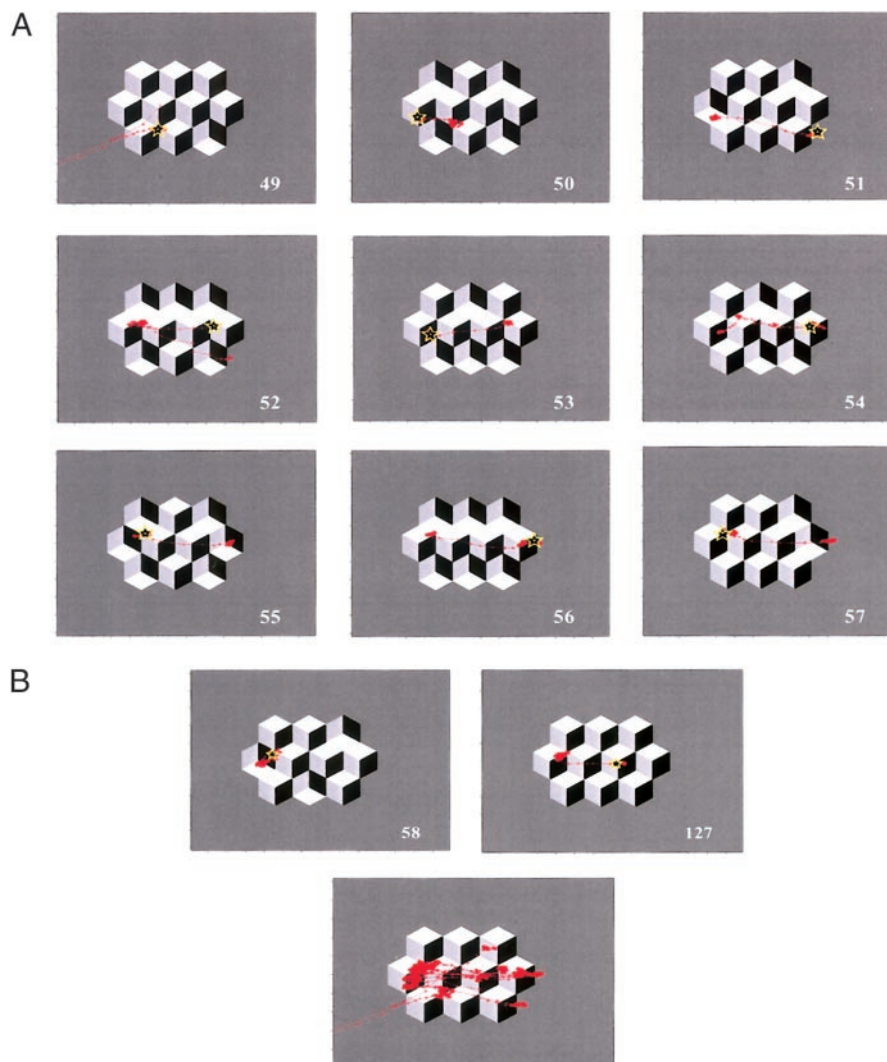
FIG. 3. Stimulus sequence and eye movement behavior from one trial. *A*: image frames 49 through 57. Each image is on screen for 500 ms. Eye positions (including both horizontal and vertical dimensions) recorded over 500 ms between transitions are superimposed on images. Screen subtends 27° horizontally and 21° vertically viewed at 114 cm. Yellow star indicates last position of eye 5 ms before next m-sequence transition. This is the same behavioral trial as illustrated in Fig. 4. Tick marks on axes of panels represent 2° of visual angle. *B*: *Top row*: image frames 58 and target (frame 127). Same conventions as in A. *Bottom row*: entire scan path for behavioral trial is superimposed on target image. Frame 127 is the image that the monkey must recognize to receive a reward at end of trial.

that the bulk of the occipital lobe EMPs in our recordings show, on average, less directional modulation (see Figs. 10 and 11) than the example presented here in Figs. 5–8. We highlight this less-typical example because it allows us to demonstrate how our methods of analysis can reveal differences in the timing and waveforms of EMPs associated with leftward and rightward saccades even when the LFPs are recorded from the same cortical location.

Characterizing the signals in detail during active vision where saccades are often made in rapid succession requires addressing a number of concerns. An averaging epoch of 1 s on either side of the saccade onset time can introduce multiple eye movement events into the pre- and postsaccadic phases of each estimate. As can be seen in Fig. 4, the rate of saccade generation is approximately 3/s. Restricting the temporal averaging window to 500 ms centered on the saccade time increases the independence of the samples. A 250-ms postsaccadic phase of neural activity is less likely to contain the presaccadic activity appearing 250 ms before the next eye movement. A 500-ms window also reduces the chance that the activity associated with undetected saccades (i.e., saccades that did not pass the automated velocity criterion comparison) will contribute to either the pre- or postsaccadic components of the LFPs. Closer inspection of Fig. 4 reveals that there was ≥1 leftward (at

about 900 ms) and 2 rightward (at about 3,800 and about 4,900 ms) small-amplitude saccades that were missed by our conservative saccadic detection algorithm in this trial alone. These 3 small-amplitude saccades probably represent fixational eye movements. They are not produced at an abnormally high rate and, as a consequence, are preceded and followed by periods of 250 ms that do not contain large-amplitude saccades. Thus these small-amplitude saccades would not have contaminated the perisaccadic intervals of the saccades obtained from this trial. As discussed in METHODS *Data analysis*, an attempt was made a priori to maximize the independence of the LFP samples by forming separate analysis categories for saccades of different directions, for consecutive saccades of the same direction, and for saccades preceded or followed by stimulus transitions.

Averages formed with 500-ms time windows are shown in Fig. 6, *A* and *B*. Here, for the purpose of demonstration, the averages for ipsiversive (rightward) and contraversive (leftward) saccades are formed from all of the saccades with no segregation based on m-sequence transition times (stimulus transients) or saccade ordering. The LFP activity associated with each saccade is shown in Fig. 6, *C* and *D*.

In the saccade-by-saccade V2 and TE Left plots (Fig. 6, *C* and *D*), 31 of 119 leftward saccades are followed by an
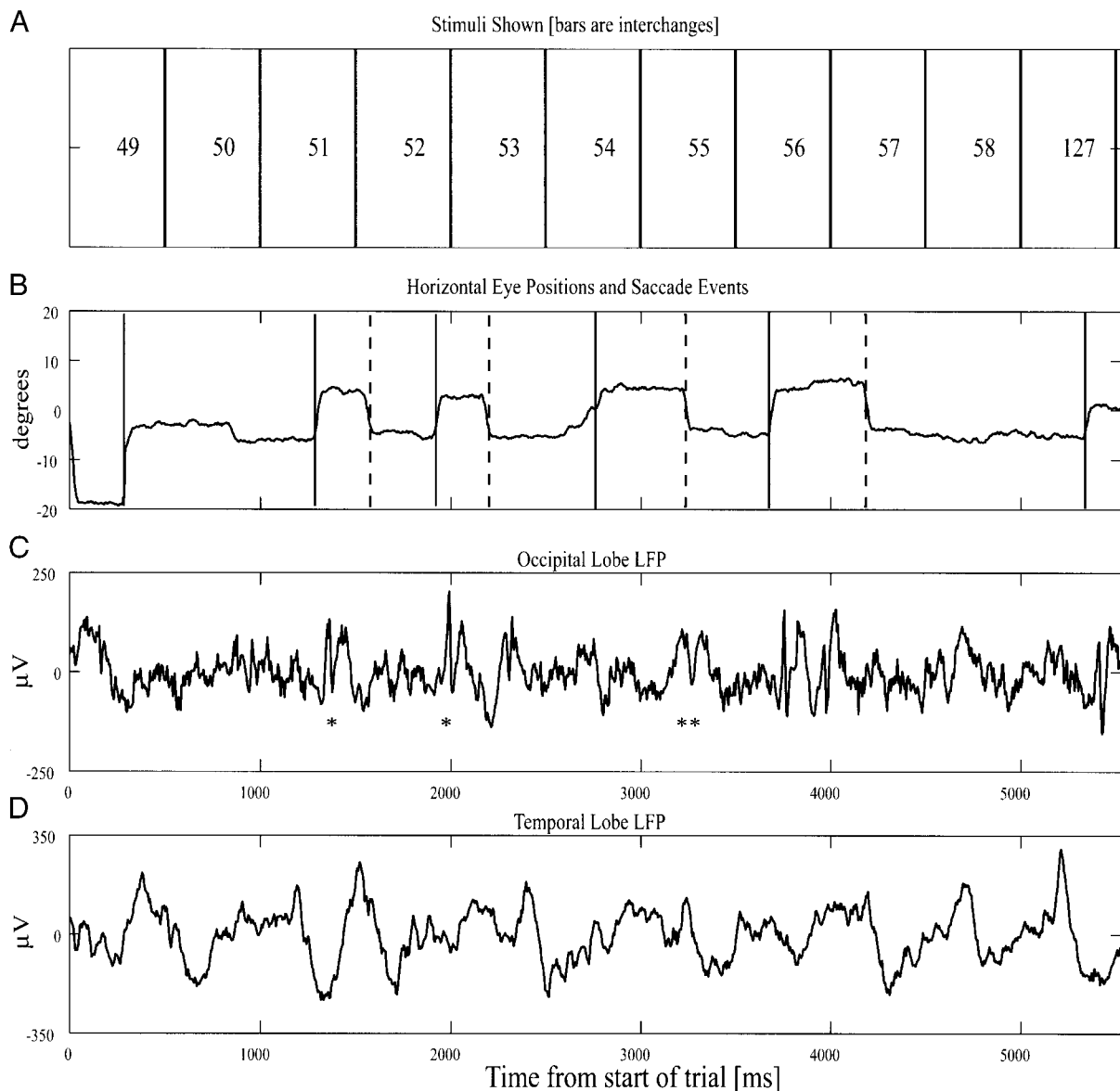
FIG. 4. Experimental events and data collected during one behavioral trial. *A*: transitions between 10 images constructed from multi-input m-sequence, and target, are shown by vertical lines. Numbers correspond to image frames (each 500 ms in duration, 2-Hz modulation rate) that appear in Fig. 3, *A* and *B*. Number 127 corresponds to target image. Presentation of target always closes out trial. Hexagonal regions do not disappear between transitions. Subregions are replaced by the next set of subregions specified by the modulation sequence outlined in Fig. 1. *B*: eye movement recording during trial. Only horizontal component is shown. Vertical lines indicate saccade onset time determined off-line by detecting a velocity that exceeds a set threshold. Note that this threshold is somewhat conservative in that a number of potential saccades, one preceding 1-s mark and again, one preceding 5-s mark, are not recognized. *Rightward saccades* (ipsiversive) are indicated by black vertical lines and *leftward saccades* are marked with dashed vertical lines. The *y*-axis is given in degrees of visual angle. *C*: local field potential (LFP) recording in occipital lobe (area V2). Asterisks indicate putative eye movement potentials (EMPs). Only a few of the EMPs are so marked. Single asterisks connote EMPs associated with rightward saccades, whereas the double asterisk shows occurrence of a leftward saccade EMP. The *y*-axis is given in units of microvolts. *D*: local field potential recording in temporal lobe (area TE). Here LFP responses to stimulus transitions are more apparent. The *y*-axis is given in units of microvolts.

m-sequence transition and a rightward saccade, with the rightward saccades having an average latency of 200 ms with respect to the stimulus transients. Fifty-three of the remaining leftward saccades are not paired with any rightward saccades. Thirty-five additional leftward saccades are paired with rightward saccades but their temporal relationship with respect to the former is more variable.

Two prominent features appear in the TE Left plot (Fig. 6*D*, *top panel*). The blue swatch in the *presaccadic* phase appears to track the stimulus transitions. However, this feature leads the m-sequence transitions by ≥50 ms. Thus the most likely source for a segment of this blue region is the LFP activity associated with rightward saccades that were generated in response to some of the stimulus transients in the postsaccadic phase of the leftward saccades. The second prominent feature in the TE left plot (Fig. 6*D*, *top panel*) is the region of positive LFP voltage values (yellow-reds) that appears to straddle the saccade onset time (0 ms) over the sample set. Because the
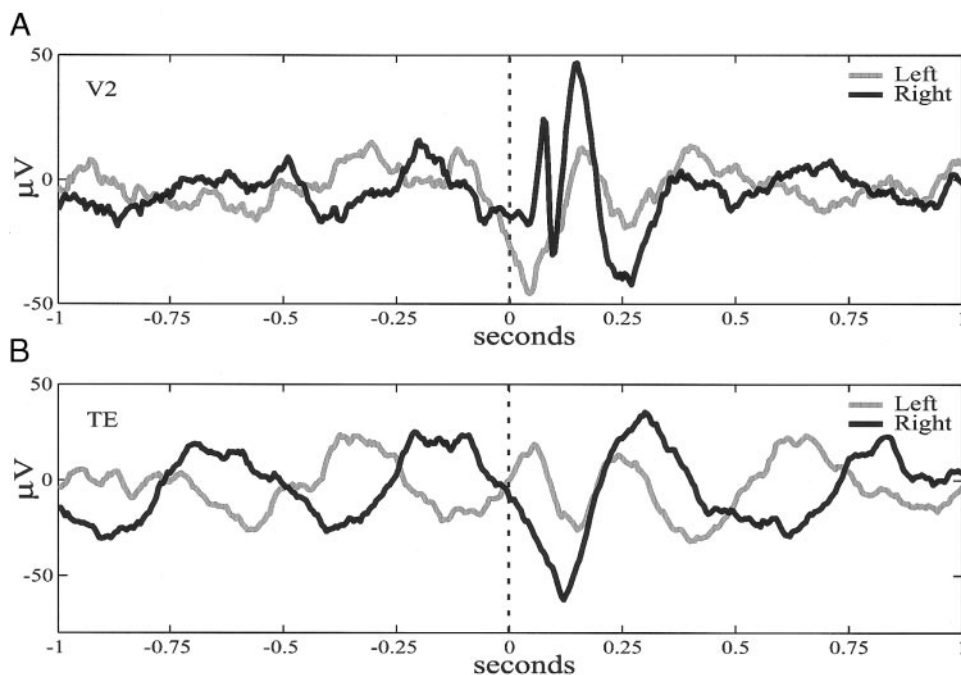
FIG. 5. Saccade-triggered averaging of local field potentials. From 54 behavioral trials, one of which is illustrated in Figs. 3 and 4, onset of 216 leftward saccades was used to form the EMP from LFPs recorded in V2 right hemisphere (*A*) and TE (*B*). The same was done with 209 rightward saccades. Averaging window used here for purpose of constructing this figure was 1 s on either side of saccade trigger.

stimulus transitions move through this region rather than delimit its onset side, it is unlikely that the positive peak in the EMP (see Fig. 6*B*, *left*) is a visually evoked potential. There may be interactions between the stimuli and saccade-related activity but these are difficult to extract from the postsaccadic components of the averages of the signals that we focus on in this study (see following text, *Interactions between visual transients and saccades*).

The extent to which the averages calculated for one particular saccade grouping parameter are distorted by the activity of oppositely directed surrounding saccades is reduced by several factors. First, putting sequential saccades with the same horizontal component (leftward, for example) into 2 separate analysis groups disrupts the "wraparound" effect seen in the saccade-by-saccade plots in the TE Left plot (Fig. 6*D*). This procedure allows for time to develop between the postsaccadic phase of one leftward saccade and the presaccadic phase of the next leftward saccade to be included in the analysis group. As a consequence, the timing of an interaction between a stimulus transition and a saccade appearing late in the postsaccadic phase of an oppositely directed saccade will tend not to reinforce a similar interaction 2 saccades away. There will be even less reinforcement of these types of interactions when the saccade groups are formed across trials. Second, the emphasis here is on estimating the EMP, and the quality of this estimate formed by using the saccade onset time as the averaging trigger. The averaging procedure reinforces the signals timed to this trigger and leads to partial cancellation of LFP components produced by oppositely directed saccades appearing in the perisaccadic interval.

Spectrograms

Time–frequency spectrograms for the average LFPs presented in Fig. 6 are shown in Fig. 7. For these spectrograms, the inputs to the spectral analysis are the averages calculated from 119 leftward saccade-referenced LFPs (Fig. 7, *A* and *C*) and 109 rightward saccade-referenced LFPs (Fig. 7, *B* and *D*). Traditionally, calculation of a spectrogram involves the subtraction of the average signal from each signal sample before computing the Fourier transform. Here we produce a time–frequency representation of the average LFP, not of the residual variance remaining after subtraction of the average. The nonzero power spectral density values in the spectrograms were established by setting a threshold based on an estimate of the standard error of the mean spectrogram (see METHODS, *Data analysis*, and APPENDIX A).

The centroids of the largest ROIs in the spectrograms in Fig. 8 are indicated by the white stars; the white circles indicate the maxima. The orientation and eccentricity of the major axis of the best-fitting ellipse to an ROI summarize the temporal waveform of the transient response in the perisaccadic interval. For example, an orientation of 90° from the vertical and an eccentricity near 1 are associated with a temporal waveform that does not sweep through frequency bands over the course of the response. The temporal waveform thus resembles a mixture of a few damped sinusoids restricted to a narrow band of frequencies (Figs. 6*B*, *leftward saccades*, and 8*C*). An orientation of 0° or 180° and an eccentricity near 1, on the other hand, indicates that the temporal waveform is more short-lived but with a much richer frequency content as is often produced by a transient response. Finally, a more oblique orientation is produced by temporal waveforms that display FM. In Fig. 6*A* (*rightward saccades*), the average LFPs exhibit a period of rapid modulation, after the saccade, that is then followed by a slower component. Note that the spectrogram for this waveform shows a frequency sweep with the largest ROI starting at higher frequencies and progressing to lower frequencies (Figs. 7*B*, 8*B*). The major axes are shown for the largest, or solitary ROIs in each part of Fig. 8. The major axes provide a useful descriptor of the temporal waveforms of the LFPs produced in the perisaccadic interval.
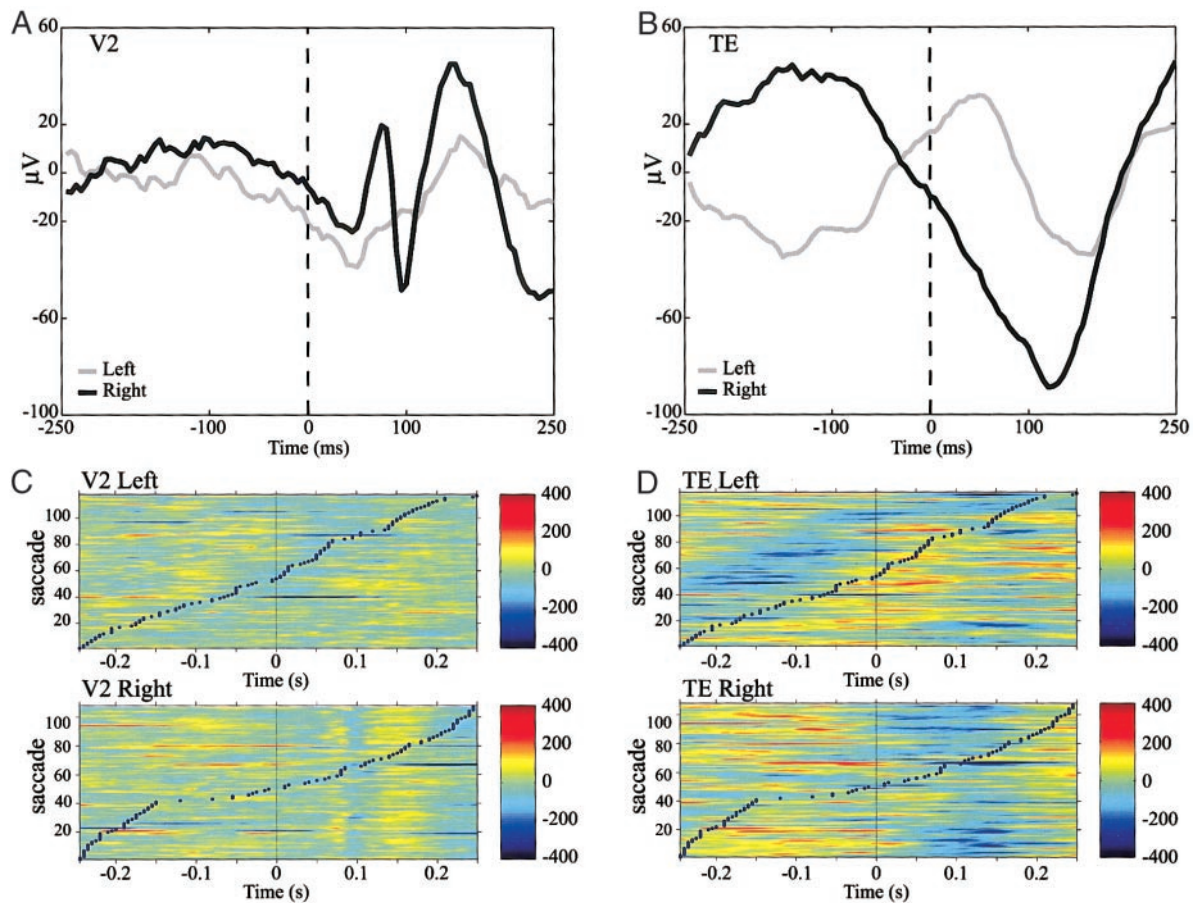
FIG. 6. EMPs in a restricted temporal window around saccades. *A*: EMPs (as LFP averages organized by saccade onset time at 0 ms) for V2 activity also displayed in Figs. 4 and 5 for 119 leftward (contraversive) saccades and 109 rightward (ipsiversive) saccades. Averaging window is restricted to 500 ms centered on onset time of saccades. Because of restrictions placed on what saccades can be included in analysis groups, in particular, that 2 saccades separated by an intersaccadic interval of <250 ms are excluded if they are either both leftward or rightward, the number of saccades is considerably less than that used for forming the EMPs shown in Fig. 5. Vertical axis ranges from −100 to 80 μV. *B*: EMPs (as average LFPs organized by saccade onset time of 0 ms) for TE activity also displayed in Figs. 2 and 4 for 119 leftward and 109 rightward saccades. Plotted ranges of voltage and time are same as in *A*. C: saccade-by-saccade plot of V2 LFPs recorded in right hemisphere. Note larger range of voltage fluctuations (−400 to +400 μV in colorbar) of individual LFPs not seen once the average is taken. Small marks that snake through field potentials are times of m-sequence interchanges (visual transients). Interchange rate for behavioral trials in this example was 2 Hz. As a consequence, there is only one stimulus transition per 500-ms window. Here saccades are ordered so that times of visual transients progress monotonically through plot with respect to opening of temporal window at −250 ms before saccade onset. *Top panel*: LFPs associated with leftward saccades. *Bottom panel*: LFPs associated with rightward saccades. *D*: saccade-by-saccade plot of TE LFPs recorded in right hemisphere. *Top panel*: LFPs associated with leftward saccades. *Bottom panel*: LFPs associated with rightward saccades.

ROI centroids and spectrogram maxima in the time–frequency plane

The numerous estimates of EMP characteristics obtained from multiple recording locations, and from saccades produced in a variety of different contexts during active vision, can be condensed into a smaller set of numbers that describe these waveforms. Figure 9 illustrates that the EMPs can populate different portions of the time–frequency plane. Here the centroids and maxima split largely over recording site. Figure 9*A* maps the time–frequency positions of the centroids of the largest ROIs extracted from the spectrograms obtained from the left and right occipital lobes during one recording session. In Fig. 9*B* the maxima of the spectrograms are mapped. For both Fig. 9*A* and Fig. 9*B*, the black disks are values extracted from left occipital cortex spectrograms, whereas the white disks are obtained from the right occipital cortex. Each disk is

from a spectrogram calculated from a unique set of LFPs defined by one of the analysis groups (see METHODS, *Grouping of saccades for analysis*, and Fig. 2). For the sake of clarity, the disks are not labeled with analysis group designators. In Fig. 9, *C* and *D* similar maps are shown for the data obtained from a right occipital lobe (V2 location in black) and right temporal lobe (TE location in white) pair recording. Examples of LFPs, EMPs, spectrograms, and ROIs drawn and composed from this data set appear in Figs. 4–8. Figure 9*C* is a map of centroids of the largest ROIs in the spectrograms and Fig. 9*D* maps the spectrogram maxima.

Other spatial relationships exist in these data and those extracted from the other recordings. An analysis of clustering in the time–frequency plane appears below in *ROI centroids and maxima in the time–frequency plane: measures of clustering*. We will show (see Fig. 9) that if the 2 channels in the data
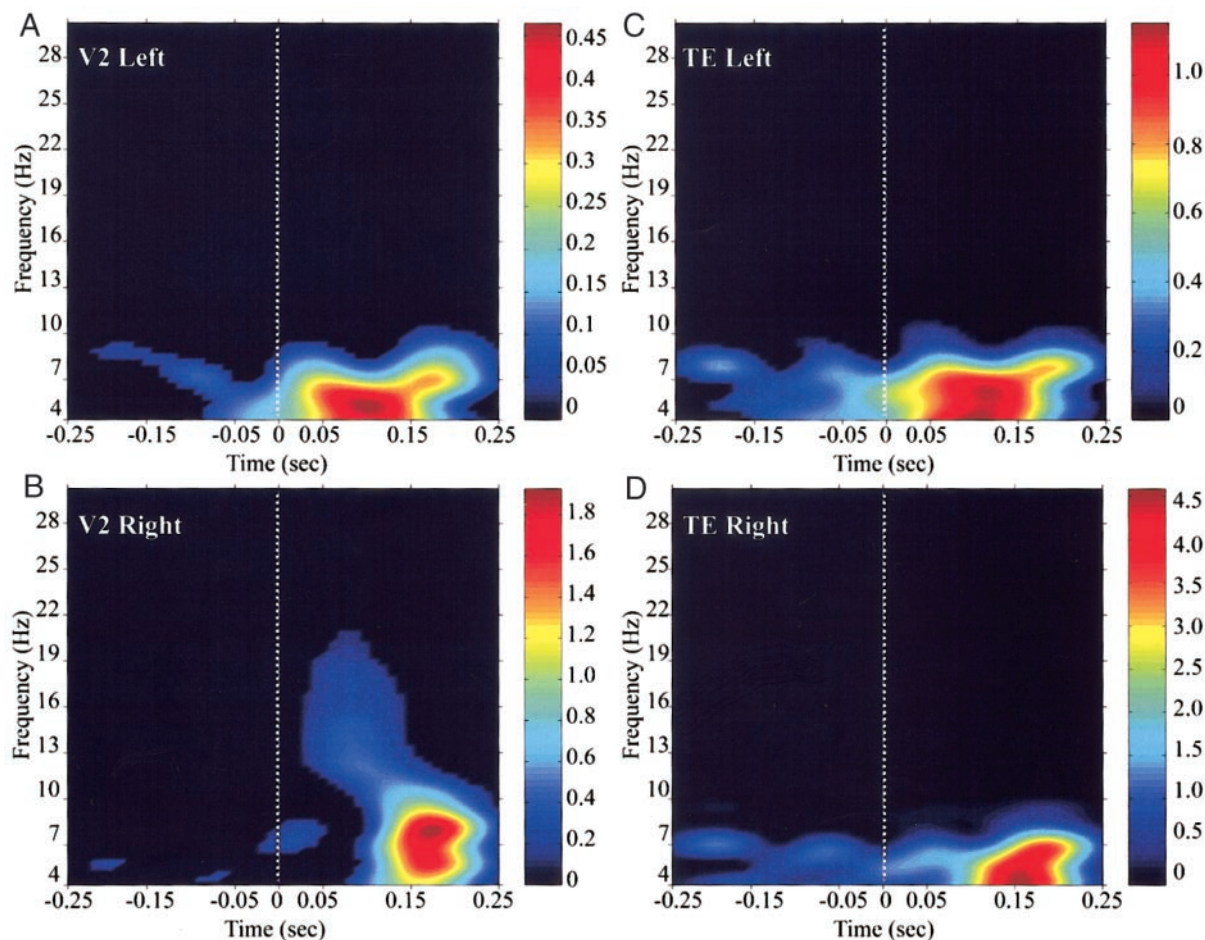
FIG. 7. Time–frequency spectrograms. Time–frequency spectrograms of EMPs presented in Fig. 6 are shown. Spectrograms of EMPs are subjected to a thresholding operation described in the text. Range of power spectral density values plotted in spectrograms is different for each panel. Units of power in spectrograms are $(\mu V)^2$/Hz (power spectral density). These units are obtained by dividing the Fourier transform of the kth-tapered LFP sample (see SUPPLEMENTS 1–3) by the square root of the Nyquist limit of digital sampling rate (200 Hz). A: EMP recorded with electrode in V2 from leftward (contraversive) saccades ($n = 119$). Peak power spectral density, 0.46 $(\mu V)^2$/Hz. B: EMP associated with rightward (ipsiversive) saccades ($n = 109$) recorded in V2. Peak power spectral density, 1.8 $(\mu V)^2$/Hz. C: spectrogram of EMP recorded in TE from leftward saccades. Peak power spectral density, 1.2 $(\mu V)^2$/Hz. D: EMP associated with rightward saccades recorded in TE. Peak power spectral density, 4.6 $(\mu V)^2$/Hz.

sets are combined, distinct clusters of centroids and maxima in the time–frequency plane can be found that are formed around the direction of the saccade. The more dramatic separation of centroids (Fig. 9C, and to a lesser extent Fig. 9A) and maxima (Fig. 9B) based on recording location, apparent from visual inspection of the positions of the black and white disks, is also reinforced by the quantitative analysis of the spatial relationships in the time–frequency plane. We will also show (Figs. 10 and 11) that if we base our analyses on the time *or* frequency positions of the centroids and maxima alone, a separation based on saccade direction will not be apparent, on average, for the occipital lobe EMPs, but will be more evident for those recorded in the temporal lobe.

Response timing and frequency content of EMPs

In Figs. 10 and 11 and in Table 1 we show that occipital and temporal lobe EMPs can be differentiated based on their timing and frequency content.

Figure 10 summarizes the positions of the centroids of the largest ROIs in the spectrograms, in time, with respect to saccade

onset, and in frequency, for all the analysis groups, runs, and recording sessions obtained for this study. Saccade directions are referenced to whether they are contraversive or ipsiversive to the recording site. Reorganizing the saccade directions by body-centered coordinates (leftward or rightward) made no significant changes to the distributions for the occipital lobe. For the temporal lobe results, no recordings were made in the left hemisphere; consequently, contraversive is synonymous with leftward and all ipsiversives are rightward saccades. The total number of centroid estimates used to produce the distributions is given in the title of each relative-frequency time histogram.

For both contraversive and ipsiversive saccades, signal power of the EMPs is centered in the postsaccadic phase of the perisaccadic interval. The range between 75 and 150 ms after saccade onset contains about 67% of the centroids associated with contraversive saccades in the occipital lobe (Fig. 10A). That same range includes about 61% of ipsiversive occipital lobe EMP centroids (Fig. 10B). The mode of both distributions is 100 ms with similar means, 73 ms for contraversive, and 78 ms for ipsiversive saccades.
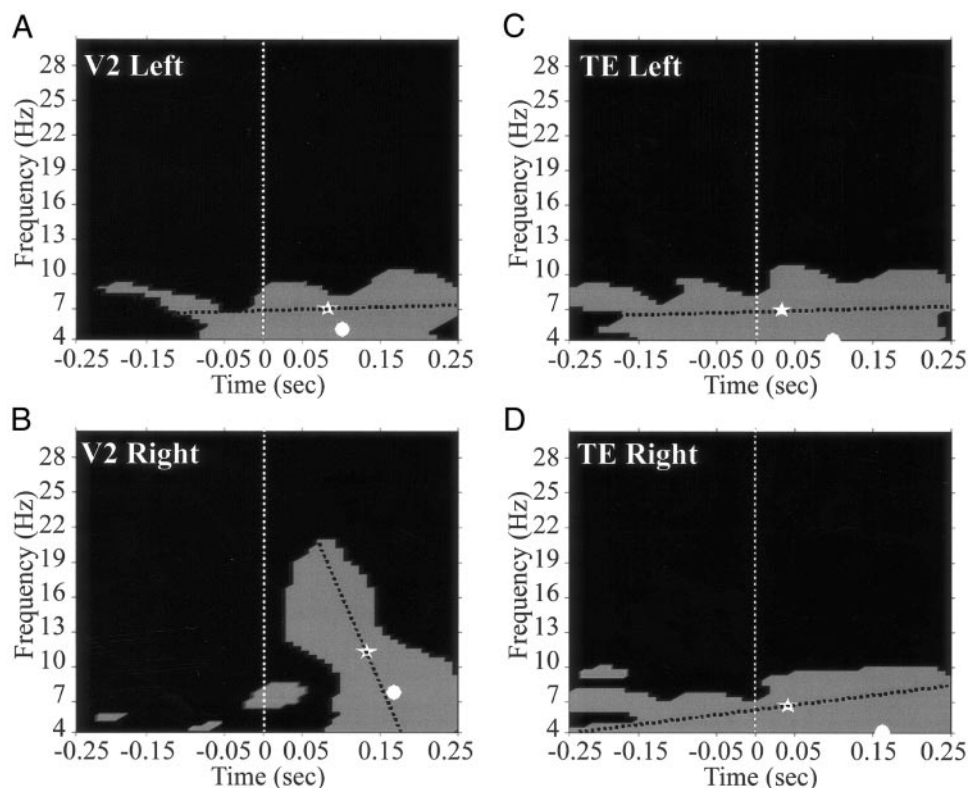
FIG. 8. Regions of interest (ROIs) extracted from time–frequency spectrograms. Panels display ROIs extracted from thresholded spectrograms presented in Fig. 7. From these regions in each spectrogram, a set of values is extracted for further analysis. *A*: V2, leftward saccade. Centroid (white star): 80 ms after saccade onset, 6.6 Hz; maximum (white circle): 100 ms, 4.7 Hz; orientation of major axis: 92°; eccentricity: 0.93. *B*: V2, rightward saccade. Centroid (white star): 130 ms, 11 Hz; maximum (white circle): 170 ms, 6.3 Hz; orientation of major axis: 20°; eccentricity: 0.94. *C*: TE, leftward saccade. Centroid (white star): 30 ms, 6.6 Hz; maximum (white half-circle): 100 ms, 4 Hz; orientation of major axis: 92°; eccentricity: 0.94. *D*: TE, rightward saccade. Centroid (white star): 40 ms, 6.3 Hz; maximum (white half-circle): 160 ms, 4 Hz; orientation of major axis: 95°; eccentricity: 0.94.

For temporal lobe EMPs, the distributions of the centroid latencies (with respect to saccade onset) of the largest ROIs are more dissimilar when comparing across direction of saccade. In Fig. 10*C*, only 30% of the centroids are clustered between 75 and 150 ms. This percentage inflates to 41% if the interval expands to 175 ms. On the other hand, for ipsiversive saccades in the temporal lobe, 53% of the centroids lie in the interval including 75 and 150 ms, and 65% are in the 75- to 175-ms postsaccadic interval. Correspondingly, the modes and means of the 2 distributions are dissimilar: modes of 0 and 150 ms for contraversive and ipsiversive saccades, respectively; means of 41 and 85 ms for contraversive and ipsiversive saccades, respectively.

The centroid distributions in time and frequency for the occipital lobe EMPs are significantly different from those compiled for the temporal lobe. Visual inspection of the temporal frequency histograms in Fig. 10 (*bottom boxes* in *A–D*) suggests that the distributions are skewed toward higher frequencies in the occipital lobe than they are in the temporal lobe. This result agrees with the picture that emerges from Figs. 7 and 8 that shows elongation of spectrogram ROIs into higher frequencies for occipital lobe EMPs. This elongation raises the centroids of the occipital lobe ROIs in the frequency dimension above those found in many temporal lobe spectrograms. Note that even though ipsiversive saccades produce EMPs in the temporal lobe that are more localized in time (Fig. 10*D*), their frequency content is about the same as that for the more temporally delocalized contraversive temporal lobe EMPs.

To more objectively evaluate the uniqueness of the centroid distributions presented in Fig. 10, the 2-sample Kolmogorov–Smirnov (KS2) test was performed (KSTEST2 in MATLAB v6.1) on each pair of distributions in the figure. The time and frequency coordinates of the centroids were evaluated separately. The hypothesis that any 2 of the centroid ensembles, such as the time values for contraversive occipital lobe centroids and their ipsiversive counterparts, were drawn from the same distribution was rejected if the *P* value obtained from the test was <0.025 (2-tailed, 95% confidence level). The results of these tests are summarized in Fig. 11.

Table 1 presents some of the values useful for characterizing the distributions shown in Fig. 10 (see Table 1 caption for details), and Fig. 11 presents the results of the KS2 tests. The "Tdist" values summarize how the distributions are balanced about saccade onset time (0 ms). "Tdist" is defined as Tdist = $[n(\text{pst}) - n(\text{pre})]/[n(\text{pst}) + n(\text{pre})]$, where $n(\text{pst})$ and $n(\text{pre})$ are the number of spectrograms that had centroids in the presaccadic and postsaccadic phase, respectively, of the perisaccadic interval. Thus if the number is 1, all of the centroids in the distribution are piled up at 250 ms in the postsaccadic phase; for −1 the concentration is at −250 ms in the presaccadic phase; and for small fractions, the centroids are then more evenly dispersed around saccade onset time. In the columns arranged below the header "Maxima" in Table 1 are values extracted from the distributions of the maxima of the spectrograms. These distributions are not shown.

The conclusions to be drawn from Table 1 and Fig. 11 are that: *1*) the direction of the saccade does not have as much influence on the activation time of the EMPs (as measured by the position of the centroids in time) in the occipital lobe recording sites as it does in the temporal lobe sites; *2*) most of the activation elicited by the saccade in the local neural population is postsaccadic in the occipital lobe, but can be either presaccadic or postsaccadic in the temporal lobe if the saccade is contraversive, and is mostly postsaccadic for
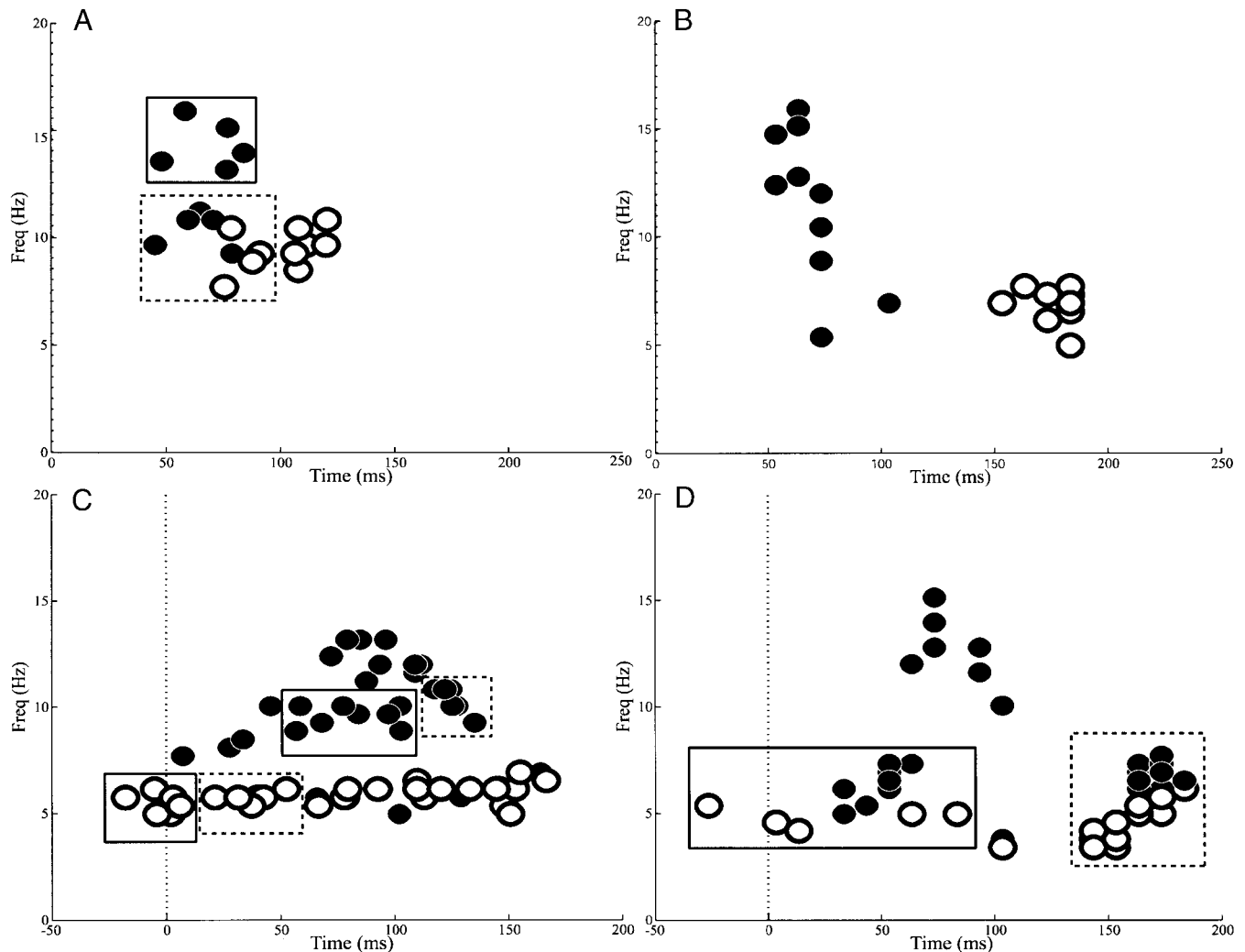
FIG. 9. Positions of spectrogram centroids and maxima in time–frequency plane. *A*: centroids of largest spectrogram ROIs from EMPs recorded simultaneously in left occipital lobe (black) and right occipital lobe (white). Each disk represents a centroid extracted from one analysis group that could be constructed from this recording session. M-sequence interchange rate was 3 Hz. Time zero on *x*-axis (0 ms), also indicated by dashed line superimposed on frequency axis, is time of saccade onset. Solid rectangle surrounds identified cluster of centroids associated only with contraversive saccades. Cluster was extracted by an algorithm described in text (*ROI centroids and maxima in the time–frequency plane: measures of clustering*) and in APPENDIX C. Dashed rectangle surrounds centroids associated with ipsiversive saccades. *B*: spectrogram maxima from same set shown in *A*. Some maxima are hidden from view because of their close proximity in time–frequency plane. No clusters for saccade direction could be found in this set of maxima. *C*: centroids of largest spectrogram ROIs from EMPs recorded simultaneously in right occipital lobe, V2 (black) and right temporal lobe, TE (white). Three m-sequence interchange rates were used in the recording session: 2, 3, and 4 Hz. Thus more independent analysis groups could be formed from this pair recording and, as a consequence, more centroids are available for evaluation. Solid rectangle in each channel of data surrounds a cluster of centroids associated only with contraversive saccades. Dashed rectangle in each recording channel surrounds centroids associated with ipsiversive saccades. Time zero on *x*-axis (0 ms), also indicated by dashed vertical line, is time of saccade onset. *D*: spectrogram maxima from same set shown in *C*. Some time–frequency maxima are hidden from view because of their close proximity in time–frequency plane. Solid rectangle surrounds identified cluster of maxima associated only with contraversive saccades. Dashed rectangle surrounds maxima associated with ipsiversive saccades.

ipsiversive saccades; *3*) the EMP waveforms are centered at 100 ms after saccade onset in the occipital lobe for both directions of saccade; *4*) temporal lobe EMPs are centered at 150 ms for ipsiversive saccades and at saccade onset (0 ms) for contraversive saccades; *5*) there are more EMPs with higher temporal frequency content in the occipital lobe than are found in the temporal lobe.

Similar conclusions can be drawn from an examination of the spectrogram maxima. Overall, the pattern of distributions that are distinguishable from one another is the same

as that found with the centroids. However, there is a general shift of the distributions of the maxima to longer latencies and lower frequencies than what is seen with the centroids (Table 1). Thus the trend is that the peak power of the EMPs comes later in the postsaccadic interval and is associated with a slower component in the waveform. A notable exception is evident for the OC spectrograms (Table 1). The maximum power in these EMPs appears 50 ms after saccade onset but the LFP activity in the EMP is centered at 100 ms after saccade onset.

TABLE 1. *Response timing and frequency content of eye movement potentials*

	Centroids				Maxima			
	OC	OI	TC	TI	OC	OI	TC	TI
Tmode (ms)	100	100	0	150	50	175	175	150
Tmean (ms)	73	78	41	85	80	88	45	100
Tdist	0.69	0.69	0.17	0.63	0.63	0.66	0.21	0.60
Fmode (Hz)	9	10	6	6	6	6	6	6
Fmean (Hz)	8.8	9.3	7.6	8.9	7.3	7.8	6.8	6.7
n	251	164	255	168	251	164	255	168

Values extracted from the centroid distributions shown in Fig. 10, *A* and *B* (columns "OC," "OI"), Fig. 10, *C* and *D* (columns, "TC," "TI"), and from the distributions of spectrogram maxima. Rows "Tmode," "Fmode," "Tmean," and "Fmean" indicate the modes of the time and frequency distributions (centroids and maxima), and means of the time and frequency distributions (centroids and maxima). "Tdist" values summarize how the distributions are balanced about saccade onset time (0 ms). "Tmode" and "Tmean" values are given in ms after saccade onset. "Fmode" and "Fmean" values are given in units of temporal frequency (cycles/s, Hz). Row "*n*" indicates the number of spectrograms that are examined for each category. Each spectrogram has a point in the time–frequency plane where the center of mass of a region of interest is located (centroids) and where the power reaches a maximum value (maxima).

Interactions between visual transients and saccades

As illustrated in Figs. 3 and 4, saccades occur during the ongoing presentation of a sequence of images. Thus the perisaccadic interval used to analyze the EMPs frequently contains a stimulus transition that appears either before or after the saccade. For 2 of the modulation rates (3 and 4 Hz), stimulus transitions can occur in both the presaccadic and postsaccadic phases of the 500-ms perisaccadic interval. Table 2 lists the modes and means extracted from distributions of ROI centroids and spectrogram maxima for EMPs with a visual transient in the presaccadic phase of the perisaccadic interval ("O1" and "T1"), in the postsaccadic phase ("O2" and "T2"), or in both presaccadic and postsaccadic phases ("O1&2" and "T1&2"). Tdist values for the centroid and maxima time distributions are also listed.

As determined by KS2 tests (test results are not plotted), the distributions of the times of the occipital and temporal lobe ROI centroids are not differentiated by the appearance of a single stimulus transient in either the presaccadic or postsaccadic interval alone. The distributions of spectrogram maxima follow a pattern similar to that of the centroids: the maximum power in the occipital lobe EMPs is shifted to the postsaccadic phase of the perisaccadic interval regardless of whether a visual transient appears before or after the saccade. This suggests that the visual transient does not interact very strongly with the saccade in the generation of the EMP. As seen in Fig. 6*C* (*bottom panel*, *rightward saccades*), the stimulus transitions move through the saccade-triggered LFPs with little impact on the time course of the voltage fluctuations in the postsaccadic phase.

When 2 stimulus transitions appear within the perisaccadic interval, however, the activation times of the occipital lobe EMPs are distributed more evenly between the pre- and postsaccadic intervals (in Table 2, Tdist = 0.59 for "O1&2" compared with values of 0.79 and 0.69 for "O1" and "O2," respectively). The KS2 tests indicate that the "O1&2" distributions are only significantly different from the "O1" distributions of centroid times ($P < 0.01$) and frequencies ($P < 0.0001$). When 2 visual transients appear in a 500-ms perisaccadic interval (3- or 4-Hz m-sequence modulation rates), their appearance within the interval is restricted to a smaller range of times than is possible with the single transients (see SUPPLEMENT 2, Fig. S*1*). The more regular timing of the double transients may thus allow for reinforcement of the visually evoked ac-

tivity in the presaccadic phase that then shifts the distribution of the activation times, and the frequency content of the EMPs toward the presaccadic phase and to higher frequencies, respectively. The visual transients appearing in the postsaccadic phase are masked by the postsaccadic concentration of power of the occipital lobe EMPs (see Fig. 10). As a consequence, the "O2" and "O1&2" distributions are not significantly different. In the temporal lobe, the distributions of the centroids and maxima are not significantly influenced by the timing of visual transients: activation times of the EMPs remain more evenly distributed about saccade onset time than those recorded in the occipital lobe EMPs regardless of the timing of the visual transients (Table 2).

Analysis of the orientation and eccentricity of the spectrogram ROIs

In Figs. 12–14 and in Table 3 we show that there are significantly more occipital lobe EMPs that exhibit FM than are seen in the temporal lobe.

The orientation and shape of the largest ROIs in the spectrograms provide a characterization of the time–frequency content of the EMPs. The orientation indicates the extent of frequency sweep in the time evolution of the LFP, whereas the eccentricity of the best-fitting ellipse suggests the extent to which the signals are equally localized or delocalized in the time and frequency dimensions. In Fig. 12, *A* and *C* the orientation of the ROIs as a function of the timing of their centroids is shown for the same recording pairs and analysis groups as shown in Fig. 9, *A* and *C*. The eccentricities of the best-fitting ellipses to the ROIs are shown in Fig. 12, *B* and *D*. Eccentricity can range in value between 2 extremes: 0 for a circle and 1 for a line.

The majority of the spectrogram ROIs extracted from the occipital lobe EMPs (white and black disks in Fig. 12*A*, black disks only in Fig. 12*C*) show a marked tendency to cluster away from the center of the range of values (90°). Contrary to this pattern, the temporal lobe orientation values in Fig. 12*C* (white disks) are more restricted to a zone around 90°. As described above, an orientation of 90° indicates that the ROI of the spectrogram shows little FM over the course of its appearance: the EMP is more like a damped sinusoid centered at a single frequency than a "chirp." As shown in these 2 panels, however, the occipital lobe ROIs have orientations placed more near 0° and 180°, indicating that their EMPs are more
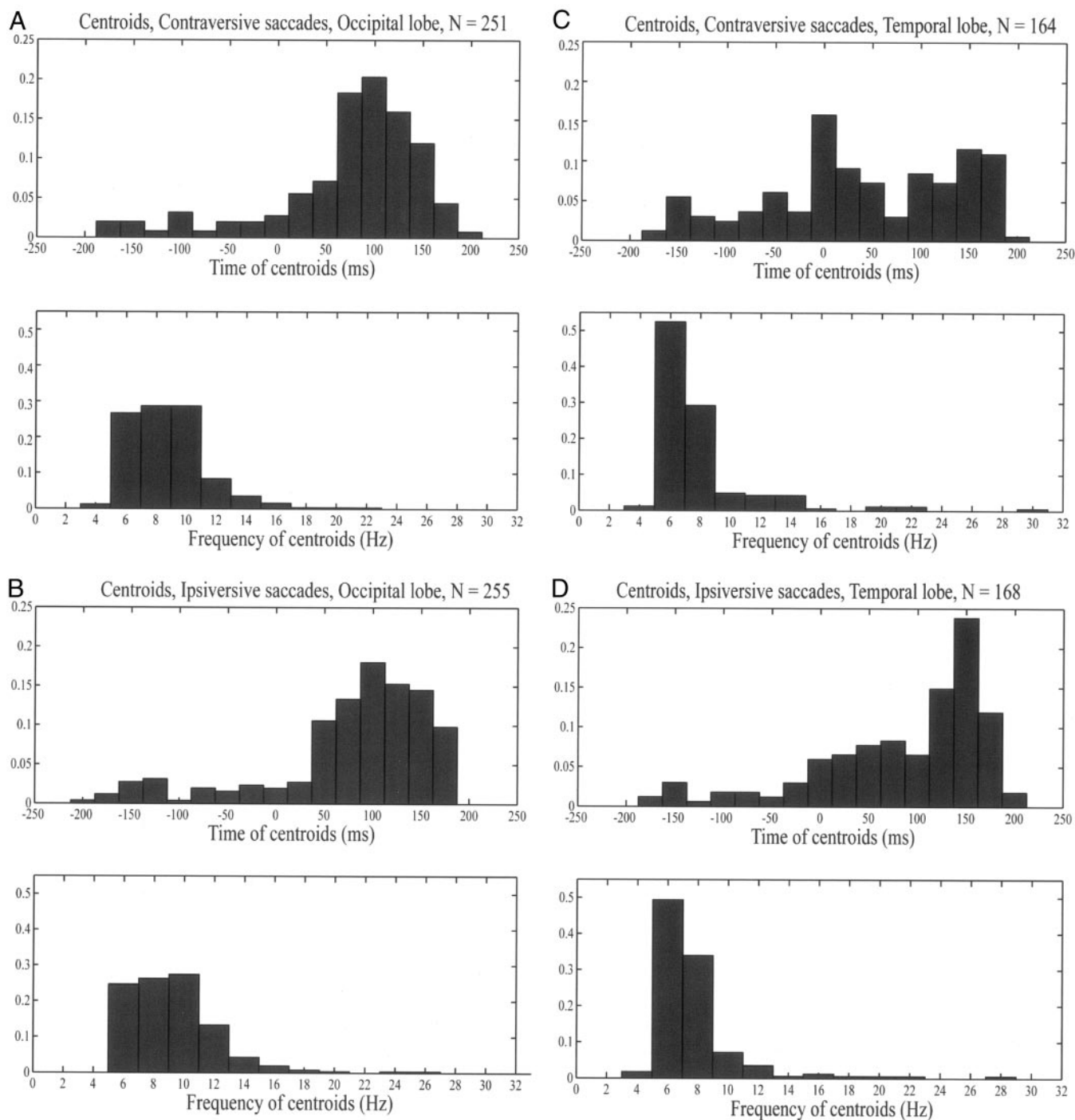
FIG. 10. Relative-frequency histograms of positions of centroids in time and frequency. *A*: distribution of centroid times (*top panel*) and frequencies (*bottom panel*) for EMPs recorded in occipital lobe associated with contraversive saccades. Number of spectrogram ROIs used to create distributions of centroid times and frequencies is *n* = 251. *B*: same as *A*, except that associated saccades are ipsiversive; *n* = 255. *C*: distribution of centroid times (*top panel*) and frequencies (*bottom panel*) for EMPs recorded in temporal lobe associated with contraversive saccades; *n* = 164. *D*: same as *C*, except that associated saccades are ipsiversive; *n* = 168.

like chirps than damped sinusoids. The eccentricity values shown in Fig. 12, *B* and *D* are, for the most part, above 0.5. This result suggests that the majority of the ROIs of the spectrograms are more elongated than circular in the time–frequency plane across many of the conditions under which the analysis groups are formed, such as direction of saccade or timing of a stimulus transient. There is a tendency for the

temporal lobe spectrogram ROIs to become more elongated in the time–frequency plane because their centroids move to longer latencies after the saccades. Because this is matched by the appearance of orientations away from 90°, the elongation is more a reflection of an increase in their frequency content than in their duration.

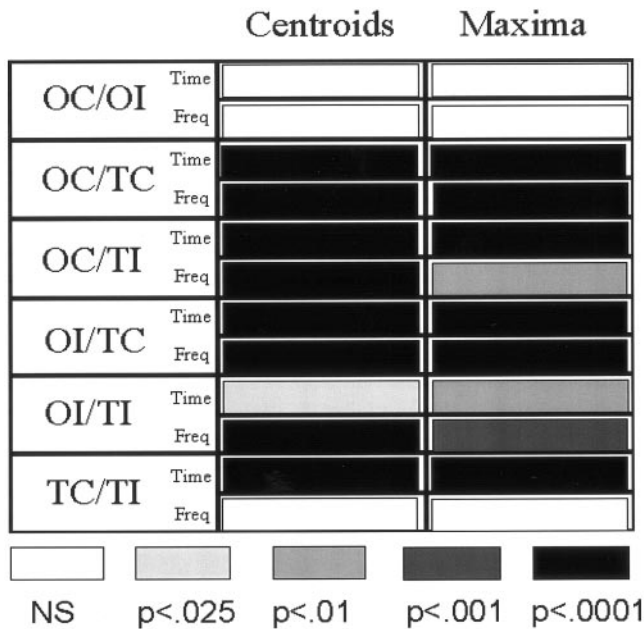Figure 13 provides a set of distributions that collect the

FIG. 11. Tests of distributions of centroids and maxima. Results of KS2 tests applied to distributions of spectrogram centroids and maxima. Tests between distributions of time and frequency values of centroids of largest ROIs are in column labeled "Centroids" with subrow headings "Time" and "Freq," respectively. Distributions from Fig. 10 are referenced by "OC," for occipital lobe centroids associated with contraversive saccades; "OI," occipital lobe centroids associated with ipsiversive saccades; "TC," for temporal lobe centroids, contraversive saccades; and "TI." for temporal lobe centroids, ipsiversive saccades. *P* values produced by tests (probability of being incorrect when rejecting null hypothesis that there is no significant difference between 2 distributions) is indicated by color of the box. White indicates that null hypothesis cannot be rejected (NS for not significant, or $P \geq 0.025$ for a 95% 2-tailed criterion), and black indicates that probability of being incorrect when rejecting null hypothesis is <1 part in 10,000. Intermediate gray colors represent other confidence levels. Column labeled "Maxima" gives results for KS2 tests performed on distributions of spectrogram maxima. For example, in row labeled "OC/OI" results of KS2 test applied to OC and OI centroid distributions are given in first column, and results of the test applied to OC and OI maxima distributions are given in the second column.

values of orientation and eccentricity extracted from all of the spectrograms. The distributions are organized around the occipital (Fig. 13, *A* and *B*) and temporal (Fig. 13, *C* and *D*) lobe recording sites, and around the direction of the associated saccades, contraversive (*A* and *C*) and ipsiversive (*B* and *D*). Figure 14 encapsulates the results of the KS2 test applied to

every pair of distributions presented in Fig. 13, separately for orientation and eccentricity. The distributions of the orientations of the temporal lobe ROIs are dominated by a mode of 90° (Table 3). This is true for both contraversive and ipsiversive saccades. The occipital lobe ROI orientations are distributed more toward values near 20°, signifying the greater prevalence of FM in these EMPs. The emergence of more weight in the distribution at 90° for the contraversive occipital lobe ROIs and at 20° for the ipsiversive temporal lobe ROIs causes these distributions to look nearly the same in the KS2 test.

ROI centroids and maxima in the time–frequency plane: measures of clustering

To further characterize the EMPs, the "spatial" relationships of the ROI centroids and spectrogram maxima in the time–frequency plane were evaluated. The analyses presented above emphasize the distribution of centroids and maxima with respect to either time or frequency. As such, the procedures constitute a form of univariate analysis. Here we consider the influence of parameters such as recording location, direction of saccade, and timing of stimulus transients on the timing *and* frequency content of the EMPs as joint-dependent variables.

The "spatial" organization of the centroids and maxima in Fig. 9 in the time–frequency plane can be evaluated using measures of distance or separation. For example, the average Euclidean distance between all of the occipital lobe centroids in the time–frequency plane in Fig. 9C can be compared against the average distance between the temporal lobe centroids. Combining the centroids from both channels of recording and ordering the distances within the set provides a means for forming clusters in the time–frequency plane in the perisaccadic interval.

A hierarchical cluster tree is formed by making successive subdivisions of the sets of centroids or maxima based on establishing the distance between the centers of mass of the 2 subdivisions. Because the algorithm follows successive binary subdivisions of the set, it is possible to define clusters involving a small fraction of the original set of values of time and frequency. The question at each stage of the algorithm is: how can the remaining unorganized data be divided into 2 clusters that maximize the distance between their centers of mass? Here the clusters are evaluated for their inclusion of groups of centroids or maxima that are delineated by the direction of the

TABLE 2. *Interactions between visual transients and saccades*

	Centroids						Maxima					
	O1	O2	O1&2	T1	T2	T1&2	O1	O2	O1&2	T1	T2	T1&2
Tmode (ms)	100	100	100	150	150	138	175	175	50	175	175	150
Tmean (ms)	89	75	63	61	60	77	89	84	78	51	77	86
Tdist	0.79	0.69	0.59	0.29	0.33	0.56	0.70	0.65	0.60	0.18	0.40	0.59
Fmode (Hz)	8	10	10	6	6	6	6	6	6	6	6	6
Fmean (Hz)	8.9	9	9	7.8	8	8	7.4	7.7	7.5	6.8	6.9	6.6
n	158	182	165	99	110	110	158	182	165	99	110	110

Values extracted from the distributions of the centroids and maxima formed around the timing of stimulus transients in the perisaccadic interval (columns "O1," "O2," "O1&2," "T1," "T2," "T1&2") under headings "Centroids" and "Maxima." Definitions for the row labels "Tmode," "Tmean," "Tdist," "Fmode," and "Fmean" are given in Table 1. "O1": occipital lobe, visual transients appear in the presaccadic phase of the perisaccadic interval. "O2": occipital lobe, visual transients appear in postsaccadic phase. "O1&2": occipital lobe, visual transients appear in both the presaccadic and postsaccadic phases. "T1": temporal lobe, presaccadic visual transients. "T2": temporal lobe, postsaccadic visual transients. "T1&2": Temporal lobe, visual transients appear in both the presaccadic and postsaccadic phases. Row "*n*" indicates the number of spectrograms that were examined in each category.

TABLE 3. *Orientation and eccentricity of spectrogram regions of interest*

	OC	OI	TC	TI	O1	O2	O1&2	T1	T2	T1&2
Orient_mode (deg)	20	20	90	90	20	20	20	90	90	90
Orient_mean (deg)	89	76	81	83	78	78	82	91	84	78
Eccen_mode	0.90	0.90	0.95	0.90	0.85	0.90	0.95	0.90	0.95	0.98
Eccen_mean	0.81	0.82	0.81	0.79	0.78	0.84	0.81	0.78	0.82	0.79
n	251	164	255	168	158	182	165	99	110	110

Values extracted from the distributions of ROI orientation and eccentricity, Fig. 13, *A* and *B* (columns "OC," "OI," rows "Orient_mode," "Orient_mean," "Eccen_mode," "Eccen_mean") and Fig. 13, *C* and *D* (columns "TC," "TI"). Values extracted from the distributions organized around the timing of the stimulus transients of the orientations and eccentricities of the best-fitting ellipses to the ROIs are also shown (columns "O1," "O2," "O1&2," "T1," "T2," "T1&2"). "Orient_mode" and "Orient_mean" values are given in degrees of rotation from the vertical (frequency axis) in the spectrograms. Thus, 0 degrees corresponds to the vertical axis and 90 degrees corresponds to the horizontal axis. The "*n*" row indicates the number of spectrograms used for producing the distributions.

saccade, the region of the cortex (occipital or temporal lobes, left occipital or right occipital), and the timing of a stimulus transient. The number of members of each group that fall into both clusters is tabulated. The likelihood of such an apportionment of the time–frequency plane appearing by chance is judged by a procedure outlined in APPENDIX C.

Clusters for saccade direction in the sets of centroids and maxima presented in Fig. 9 are indicated by the rectangles. For Fig. 9*A*, the cluster centered in higher temporal frequencies (enclosed by the closed-line rectangle) is for contraversive saccades, whereas that for ipsiversive saccades (dashed-line rectangle) is centered at lower frequencies.
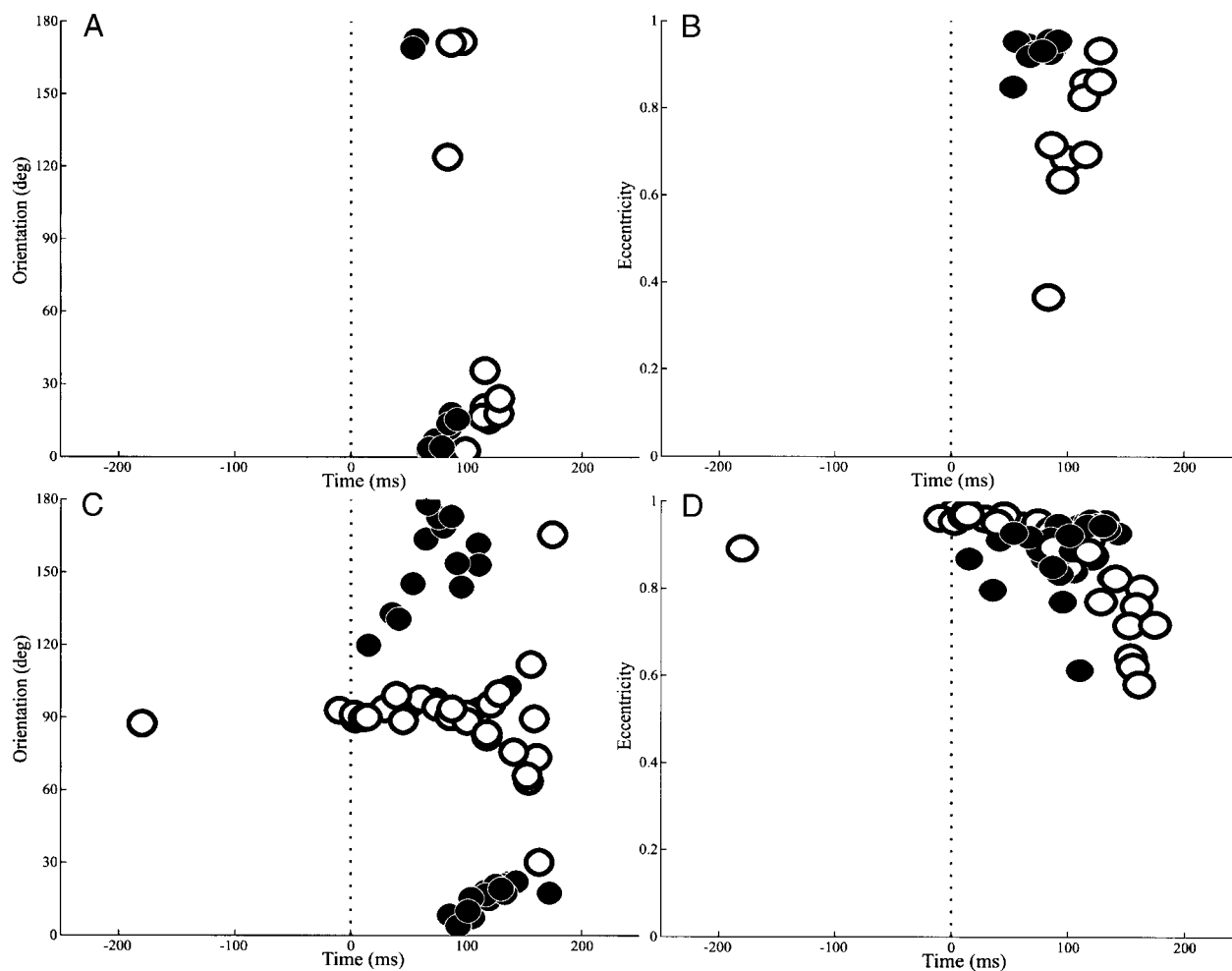

FIG. 12.   Orientations and eccentricities in perisaccadic interval of best-fitting ellipses to largest ROIs in a set of spectrograms. *A*: each disk plots orientation of major axis of best-fitting ellipse to largest ROI (*y*-axis) against time of ROI's centroid (*x*-axis). Time zero is saccade onset time. Black disks: left occipital lobe data (also presented in Fig. 9, *A* and *B*). White disks: right occipital lobe data (also shown in Fig. 9, *A* and *B*). Time zero on *x*-axis (0 ms) is saccade onset time. *B*: each disk plots eccentricity of best-fitting ellipse to largest ROI (*y*-axis) against time of ROI's centroid (*x*-axis). Black disks: left occipital lobe data (corresponding orientations presented in *A*). White disks: right occipital lobe data. *C*: orientations of major axes of best-fitting ellipses fit to largest ROIs from EMPs recorded simultaneously in right occipital lobe, V2 (black, a subset of related time–frequency values are presented in Fig. 9, *C* and *D*), and right temporal lobe, TE (white, a subset of related time–frequency values are also presented in Fig. 9, *C* and *D*). *D*: eccentricities of best-fitting ellipses fit to largest ROIs from EMPs recorded as in *C*.
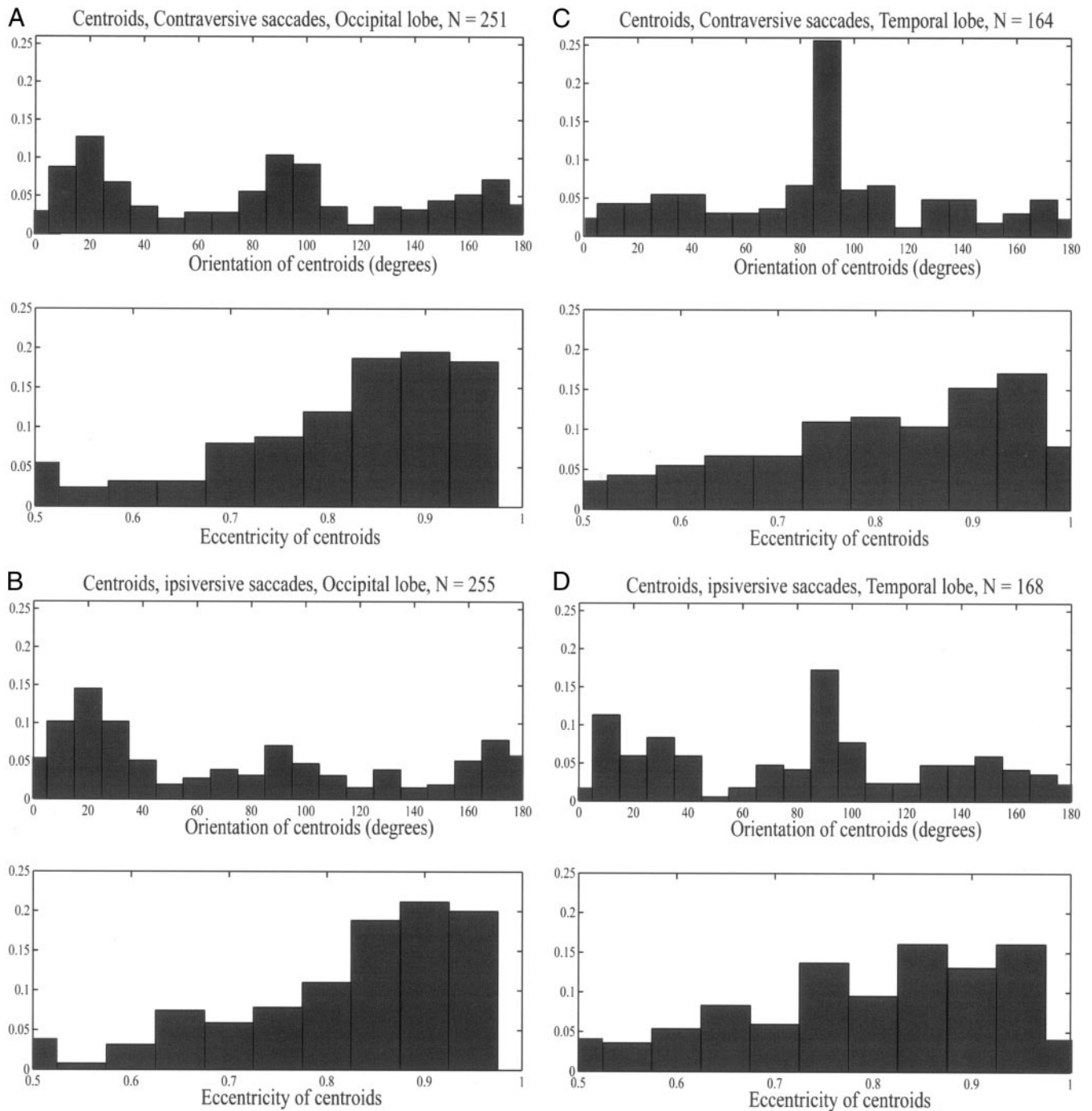
FIG. 13.   Relative-frequency histograms of orientations and eccentricities of spectrogram ROIs. *A*: distribution of orientations (*top panel*) and eccentricities (*bottom panel*) of best-fitting ellipses of spectrogram ROIs calculated for EMPs recorded in occipital lobe around onset of contraversive saccades. *B*: same as *A*, except that onset was around ipsiversive saccades. *C*: distribution of orientations (*top panel*) and eccentricities (*bottom panel*) of best-fitting ellipses of spectrogram ROIs calculated for EMPs recorded in temporal lobe around onset of contraversive saccades. *D*: same as *C*, except that averaging trigger was the onset of ipsiversive saccades.

Note that the lower temporal frequency cluster involves centroids extracted from both recording locations. This is also the case in Fig. 9*D*. In Fig. 9*C*, the clusters do not mix occipital and temporal lobe EMPs, but although significant, the clusters represent a relatively small subset of the total range of time–frequency values exhibited by the EMPs generated during the scan paths for this particular recording.

The maxima in Fig. 9*B* could not be segregated by saccade direction.

Table 4 presents the number of pair recordings that show evidence for clustering. From Table 4 we see that different cortical sites have dissimilar EMP waveforms in nearly half of the pair recordings. About 24–30% of pair recordings (centroids–maxima) have directional EMPs, with different time–
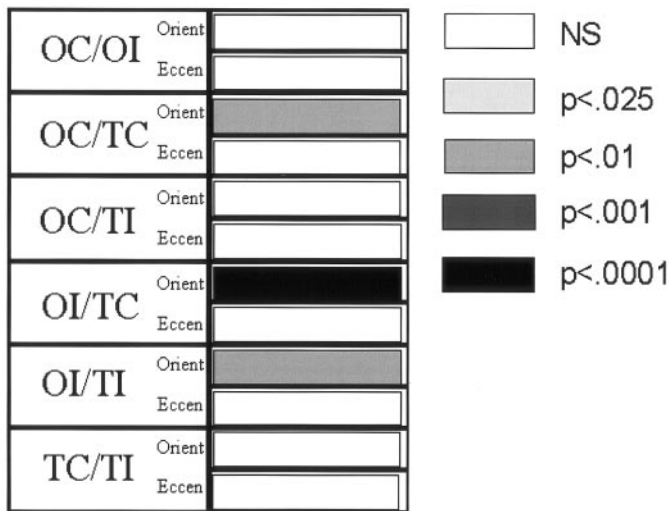
FIG. 14. Orientation and eccentricity of largest ROIs in spectrograms. Results of KS2 tests applied to distributions of orientations and eccentricities of best-fitting ellipses to largest ROIs in spectrograms. Color scheme same as in Fig. 11. Distributions are shown in Fig. 13. First row labeled "OC/OI" shows that distributions of orientations and eccentricities are not significantly different for contraversive and ipsiversive saccades, suggesting that the types of frequency modulation (FM) exhibited by EMPs in occipital lobe are identical, on average, regardless of direction of saccade.

frequency content for ipsiversive and contraversive saccades. Finally, the timing of the stimulus transient with respect to saccade onset produces significant clustering in time–frequency in only 5 out of the 34 pair recordings.

In Table 4 and Fig. 9, if we had required that clusters for saccade direction be formed from either one channel or the other, there would be much less evidence for directional EMPs. If we consider only the distribution of time values separately from those of the frequency coordinates in the time–frequency plane, as we do in the univariate analysis in Figs. 10 and 11, the evidence for directional EMPs is significantly reduced for the occipital lobe. Nonetheless, there are striking individual examples of directional EMPs in our occipital lobe recordings (Figs. 5–8, S1–S2). Directional corollary oculomotor inputs may be less uniformly distributed to the occipital lobe than they are in the temporal lobe, and therefore directional EMPs may be more difficult to encounter in the occipital lobe without targeting specialized regions of the cortex.

Summary

EMPs in the occipital lobe are largely postsaccadic events. The modes of the distributions of activation times (as measured by the centroids) are 100 ms after saccade onset regardless of saccade direction. In the temporal lobe, EMPs are both presaccadic and postsaccadic events if the saccades are contraversive. If the saccades are ipsiversive, the temporal lobe EMPs are almost entirely postsaccadic events and are concentrated at a later time in the postsaccadic interval than those generated in the occipital lobe. The frequencies incorporated into the temporal lobe EMPs are also in a lower band than those in the occipital lobe, regardless of the direction of the saccade.

Both contraversive and ipsiversive saccades produce time–frequency "chirps" in occipital lobe EMPs. Ipsiversive and contraversive saccades produce somewhat different degrees of

FM in the temporal lobe EMPs. Contraversive saccades are associated with temporal lobe EMPs that are more like damped sinusoids centered at one frequency, whereas ipsiversive saccades produce some temporal lobe EMPs that undergo a sweep through several frequencies.

Saccades with 2 stimulus transitions (at 3 and 4 Hz) in their perisaccadic intervals are associated with occipital lobe EMPs that shift somewhat toward the presaccadic phase of the intervals. The majority of the occipital EMPs, however, are centered in the postsaccadic phase regardless of the timing of external visual transients.

Centroids and maxima can be segregated in the time–frequency plane by recording location in about half of the recording pairs. Saccade direction and the timing of stimulus transitions in the perisaccadic interval also produce distinct clusters for the OT pathway as a whole, although these clusters were not as robustly represented in our data sets as those based on cortical region.

DISCUSSION

Corollary oculomotor activity in the OT pathway

For primate vision to work, the internal representation of the visual world must be assembled across numerous shifts of gaze. It has long been conjectured that fast eye movements (saccades) are associated with a corollary discharge that reports to visual processing centers information about the eye movement, including the duration (amplitude) and direction of the saccade (reviewed in Sommer and Wurtz 2002). This corollary discharge may appear around the time of each eye movement to shift and reinterpret the activity in the multiple retinotopic maps that are distributed throughout the OT pathway (reviewed in Andersen et al. 1993). It may also play a role in reducing the blur signal produced by the movement of the retina across the visual scene during the saccade (reviewed in Krekelberg et al. 2003 and McCloskey 1981). Although protecting the observer from experiencing frequent bouts of visual smear, this corollary activity may also contribute to a loss of sensitivity during the saccade (reviewed in Krekelberg et al. 2003; Niemeier et al. 2003; Ross et al. 2001; Thiele et al. 2002) and to impairments in judgment of target position (Morrone et al. 1997), spatial relationships (Cai et al. 1997), and timing (Yarrow et al. 2001) in the perisaccadic interval. A retinal contribution to the suppression of activity during saccades has been recently identified (Ölveczky et al. 2003; Roska and Werblin 2003).

Active vision, therefore, places the neural operations of visual processing in an oculomotor context. If the time between saccades is long enough, the responses of single visual neurons to a flashed stimulus are nearly identical to those seen during

TABLE 4. *Number of pair recordings with clusters in the time–frequency plane*

Cluster Variable	Centroids (total = 34)	Maxima (total = 34)
Recording location	17	15
Direction of saccade	8	10
Timing of stimulus transient	5	5

See APPENDIX C for details.

periods of prolonged fixation (DiCarlo and Maunsell 2000). However, when a rapid sequence of saccades is used in a visual task, such as the pattern-recognition task studied here, then the neural activity produced in the ventral stream must reflect both the analysis of the spatiotemporal patterns of contrast appearing on the retina and the oculomotor behavior framing the capture of visual information (Gallant et al. 1998; Gawne and Woods 2003; Richmond et al. 1999).

The question we have addressed here is, can the EMPs recorded in the OT pathway be considered as products of the activity generated in the distributed oculomotor network in the primate brain, or alternatively, do they only reflect visual activity in the retinogeniculate pathway?

Occipital lobe EMPs

Because the occipital lobe EMPs are largely postsaccadic events that are not commonly influenced by saccade direction, it is difficult to associate them with the corollary oculomotor activity that may be responsible for saccade preparation and receptive field remapping. The EMPs could represent the visual reafference that arrives at the cortex after the saccade. However, there are potential sources for postsaccadic activation from within the oculomotor network. Corticocortical projections originating in the parietal and frontal lobes are known to terminate in extrastriate visual cortex (Leichnetz and Goldberg 1988). Parietal and frontal regions demonstrate robust postsaccadic single-unit activity that is tuned for saccade amplitude and direction [inferior parietal lobule 7a: Barash et al. 1991a; FEF: Bruce and Goldberg 1985; prefrontal cortex (PFC): Funahashi et al. 1989; supplementary motor area (SMA): Schall 1991]. Suppression after refixation is also observed (FEF: Bruce 1990), and a withdrawal of excitatory inputs could contribute to the LFP activity seen in the occipital lobe. "Pause-rebound" units in SMA (Schall 1991) neurons that are transiently silenced during a saccade produce a burst of activity at the start of the next fixation. Thus the rebound, postsaccadic phase of the SMA responses could also play a role in the generation of the postsaccadic phase of the occipital lobe EMPs.

Although top-down corticocortical projections to the occipital lobe from oculomotor centers in the cortex may play a role in shaping the occipital lobe EMPs, the perisaccadic activity in the thalamus may also be crucial, and perhaps of more importance, given the less dramatic influence of saccade direction on LGN perisaccadic activity. As reviewed above, studies of LFP and both single-unit and intracellular recordings in the LGN of monkeys and cats over the last 30 yr have demonstrated the presence of robust eye movement–related activity in the thalamus (see also Hu et al. 1989; Ramcharan et al. 2001), even in the absence of retinal stimulation (Lee and Malpeli 1998). Recently, a detailed analysis of single-unit responses of alert monkey LGN neurons has confirmed the presence of an extraretinal signal in the thalamus (Reppas et al. 2002). This extraretinal signal interacts with retinal activity to produce an envelope of neural discharge that evolves from an initial phase of presaccadic-to-transsaccadic suppression to a period of excitation peaking in the postsaccadic phase at about 75–100 ms after onset of the saccade. This eye movement–related pause-rebound single-unit activity can be found in both the magnocellular and parvocellular layers of the LGN, but different

visual environments are required to enhance the postsaccadic excitation in the different populations.

The overall envelope of saccade-related activity in the monkey LGN overlaps with the time course of the EMPs we observe in the occipital lobe. It is possible therefore that the EMP activity observed in the occipital lobe represents the impact of saccade-related thalamic activation on the visual cortex. Although the modes and means of the centroids of the spectrogram ROIs are shifted to longer latencies than the thalamic activity (by 10–30 ms), intracortical processing likely adds additional delays to the wave of excitation emerging from the thalamus.

The participation of the thalamus in generating EMPs in the cortex may extend beyond the LGN. Pause-rebound activation associated with saccades, but that is neither tuned for the direction or amplitude of the eye movement, has been described in the central lateral and paracentral nucleus of the intralaminar nuclei (ILN) (Schlag and Schlag-Rey 1984; Schlag-Rey and Schlag 1984) and in the inferior and medial pulvinar of the monkey (Robinson et al. 1986). The time course and range of changes in activity levels of these single-unit responses resemble those seen in the monkey LGN. The pulvinar in the monkey is well situated to broadcast its postsaccadic rebound discharge simultaneously to multiple targets in both striate and early extrastriate visual cortex. Reciprocal projections are present between the inferior pulvinar and V4 (Adams et al. 2000; Bender 1981; Shipp 2001; Ungerleider et al. 1983) and V2 and V3 (Adams et al. 2000; Shipp 2001). Striate cortex has connections with the more lateral divisions of the inferior pulvinar (Benevento and Rezak 1976; Gutierrez and Cusick 1997; Ungerleider et al. 1983).

The burst phase of the pause-rebound (pause-burst) activation in the LGN, pulvinar, and ILN could be a crucial component of the sequence of events leading to synchronized activation of more than one cortical laminae (Swadlow et al. 2002). The anatomical range of the cortical projections of the thalamic nuclei may distribute this synchronization across a number of cortical areas at the time of saccade onset. The bursts originating in a number of thalamic nuclei could lead to the production of the postsaccadic EMPs because rebound excitation in the thalamus plays a crucial role in triggering postinhibitory rebound excitation in the cortex (Grenier et al. 1998).

The results we present here and the studies we have reviewed suggest that the EMPs in the occipital lobe reflect the action of corollary oculomotor signals, where the site of extraretinal influence is in the thalamus. As such, the EMPs in the occipital lobe may be produced by cortical responses to retinogeniculate and thalamocortical activity that is modulated at the time of the saccade. Thus the occipital lobe EMPs may be generated by activity that is more akin to an exafference signal, a signal that combines visual reafference generated during the saccade, the retinal activity generated at the start of the new period of fixation, and an oculomotor corollary discharge (McCloskey 1981). Even if this exafference signal is removed by synaptic depression at the input layers of the striate (Carandini et al. 2002; Freeman et al. 2002) and extrastriate cortex, the transient depression may itself produce a brief synchronization in small populations of cortical neurons and thereby contribute to the generation of a field potential at the time of a saccade.

Temporal lobe EMPs

We report here that the temporal lobe sites in the right hemisphere have EMPs that are distributed more equally across the perisaccadic interval for contraversive saccades than for ipsiversive saccades. Thus unlike in the occipital lobe there is significant directional tuning of the EMPs in the temporal lobe. Sobotka and coworkers earlier demonstrated evidence for tuning for the direction of saccades in LFP (Sobotka and Ringo 1997) and single-unit recordings (Sobotka et al. 1997) in the medial temporal lobe. Two of their 16 LFP recordings had postsaccadic EMPs with significantly different waveforms associated with different saccade directions, and 17% of their single units displayed a similar sensitivity.

The presaccadic signals we see in the temporal lobe could represent neural activity involved in the preparation to make a saccade. In dorsal oculomotor areas of the cortex, the presaccadic activity appears to be involved in a number of functions: *1*) target selection (seen in LIP: Gottlieb 2002; Gottlieb et al. 1998; and FEF: Schall and Hanes 1993; Schall and Thompson 1999); *2*) tuning movement fields for direction and amplitude of intended saccades (seen in LIP: Barash et al. 1991a,b; FEF: Bruce and Goldberg 1985); *3*) predictive remapping of retinotopic coordinates (seen in LIP: Colby et al. 1995; Duhamel et al. 1992; FEF: Umeno and Goldberg 1997); *4*) coregistration of retinotopic coordinates with extraretinal coordinates (seen in LIP: Andersen 1997); *5*) establishing a delay-period activity during mnemonic tasks (seen in LIP: Gnadt and Andersen 1988; Pesaran et al. 2002; FEF: Bruce and Goldberg 1985; PFC: Funahashi et al. 1989). Because LIP and FEF are either mono- or disynaptically connected with the posterior inferotemporal cortex (Webster et al. 1994), it is possible that the presaccadic activity appearing in these parietal and frontal regions could play an important role in generating the local population activity we see in the temporal lobe.

However, why should more presaccadic activity be apparent in the temporal lobe for contraversive saccades than for ipsiversive saccades? That is, why should the temporal lobe be under the control of corollary oculomotor activity for only one saccade direction?

Some of the saccades in the scan paths exhibited by the monkeys (Figs. 3 and 4) can be associated with specific visual events in the trials. This was demonstrated by calculating the reverse correlation between the times of saccade onset and the m-sequence controlling the transitions in the visual display (Kalik et al. 1999): a subset of the saccades was significantly correlated with transitions at a number of locations, in particular, leftward saccades with position 2 in the array of hexagons (see Fig. 1*C*) for monkey M, at a latency just greater than one transition time (250, 333, or 500 ms). Thus for monkey M, the positions of fixation at the end of the saccades tended to place most of the image largely in the right or left visual hemifield. As a consequence, parafoveal receptive fields in striate and extrastriate areas of opposite hemispheres may detect transitions on different sides of the visual stimulus. The presaccadic activity we see in the temporal lobe of the right hemisphere before leftward saccades may be a reflection, in part, of an orienting response to the detection of a stimulus transition in the left visual field that is not at the current focus of processing.

Two attentional systems are available to visual information processing in the primate brain (reviewed in Corbetta and Shulman 2002). The first system involves bilaterally distributed cortical areas in the dorsoparietal frontal eye field and dorsolateral prefrontal cortex. This network organizes top-down control, selecting targets for focal processing as part of goal-directed behaviors. The second system, which in humans is lateralized to the right hemisphere, includes cortical areas at the junction between the parietal and temporal lobes as well as in the ventral frontal cortex. This network is activated by salient or unexpected events not at the current focus of processing, in any sensory modality. The network acts as a "circuit breaker" (Corbetta and Shulman 2002) to the dorsal system, allowing for a shift to a new focus of processing. This shift often includes a saccade.

In our studies, EMPs recorded in the right hemisphere of the temporal lobe associated with leftward saccades may be more presaccadic because this activity reflects the generation of executive commands issued from the FEF to make contraversive saccades as part of a scan path strategy, in addition to the operation of the attentional circuit breaker. Although in humans it is possible that similar presaccadic activity should be present in the temporal lobe for ipsiversive (rightward) saccades, their diminished number in our recordings may be a consequence of the lack of hemispheric specialization in the monkey. That is, rightward saccades may be preceded by more presaccadic EMPs if the recordings were made in the left temporal lobe. The late, postsaccadic EMP activity seen in our temporal lobe recordings associated with ipsiversive saccades may reflect the EMPs passed up from occipital lobe sites to the temporal lobe through corticocortical pathways.

Frequency sweeps in EMPs

As shown in Figs. 7, 8, 12, and 13 and Table 3, the occipital lobe EMPs exhibit a greater degree of frequency sweep (transitions between frequencies in the spectrograms) during their time course than those recorded in the temporal lobe. A greater degree of frequency sweep in the spectrogram translates to a waveform that either speeds up or slows down its modulation during its time course (Fig. 6*A*, *rightward saccades*, Figs. 7*B* and 8*B*).

In the visual cortex (Shao and Burkhalter 1999), electrical stimulation of feedforward, interlaminar, and horizontal connections produces membrane potential waveforms that undergo FM in supragranular layer pyramidal cells. Activation of corticocortical feedback, on the other hand, produces enough polysynaptic excitatory postsynaptic potentials (EPSPs) to mask the inhibitory postsynaptic potentials (IPSPs) (Burkhalter 2002). Unlike feedforward activation, intracellular waveforms produced by feedback activation will exhibit less FM and reflect only the residual depolarization produced by the synaptic barrage. Thus a local field potential recording made in the cortex should be mostly monophasic (less rich in frequency content) after synaptic activation by corticocortical feedback and more frequency modulated when driven by feedforward pathways.

Our interpretation of the LFPs in terms of the dynamics of synaptic and intracellular events is derived in part from studies of the LGN where intracellular recordings were made simultaneously with extracellular field potentials (Hu et al. 1989). Monophasic negative-going extracellular field potentials, with a smooth return toward the baseline, are coincident with tran-

sient (about 150 ms in duration) depolarization of thalamic relay neurons. When a positive-going deflection briefly interrupts the negative-going field potential, an IPSP is seen in the simultaneously recorded intracellular potential. A second, slower positive-going deflection often appears after the negative field potential recovers and this phase is coincident with a more slowly developing IPSP in the intracellular recordings.

If an interpretation about synaptic and intracellular events can be extrapolated from LFPs, then the work of Burkhalter suggests that ipsiversive saccades are followed by activation of interareal feedforward and local connections in the cortex. This conclusion is based on the predominance of frequency-modulated field potentials in the postsaccadic phase of the perisaccadic interval in both occipital and temporal lobe recordings. The greater prevalence in the temporal lobe of EMPs with simpler temporal waveforms (inferred from the small degree of frequency sweep in their spectrograms) suggests that the temporal lobe receives more feedback input around the time of a contraversive saccade than does the occipital lobe. Ipsiversive saccades generate temporal lobe EMPs that take on more of the dynamics associated with the activation of feedforward pathways in the occipital lobe.

The analysis of the frequency sweeps in the ROIs of the spectrograms reinforces our interpretation of the EMPs discussed above. The occipital lobe EMPs, which we suggest are dominated by saccade-modulated activity in retinogeniculate and thalamocortical pathways, have similar dynamics to the activity in local cortical populations produced by feedforward pathways. The temporal lobe EMPs associated with contraversive saccades appear to have the right timing to be related to corollary oculomotor activity. These EMPs have similar dynamics to the activity generated by feedback pathways.

In this report, to conclude, we describe a methodology for characterizing eye movement potentials (EMPs) recorded from pairs of locations in the occipitotemporal (OT) pathway of alert monkeys performing a pattern-recognition task. Using this methodology, we establish regional differences in the activation time, frequency content, and waveforms of the EMPs. We also find that saccade direction influences cortical EMPs differently in the occipital and temporal lobes of the monkey. Our results suggest that the EMPs in the OT pathway are signatures of the corollary signals that are generated in the distributed oculomotor network at the time of each saccade. In the occipital lobe, these corollary signals are injected subcortically into the retinogeniculate and thalamocortical pathways and as such become combined with sensory afferent activity. In the temporal lobe, the corollary signals are combined with mechanisms of attention and executive control and appear first at the level of the cortex. The corollary signals create an oculomotor context for visual information processing in the OT pathway. An oculomotor context may play a role in building representations from multiple fixations (Wallenstein et al. 1998) and in the formation or dissolution of visual working memory traces in the temporal lobe (Sobotka et al. 2002) and prefrontal cortex (Gutkin et al. 2000). Analysis of the coherence between the population activities in the occipital and temporal lobes and a detailed examination of single-unit responses in the perisaccadic interval will further elucidate how such corollary oculomotor signals impact local cortical circuits, corticocortical communication, and their role in active vision.

APPENDIX A

An estimate of a statistic, such as a mean or a spectrogram, relies on a set of independent samples of data $\{X_1, X_2, \ldots, X_M\}$ from M trials (M saccades in our analysis) where each X_i can be a vector or an array. For the jackknife procedure, we form new sets of data samples that contain all of the original trials except one. For example, $\theta_1 = \{X_2, X_3, \ldots, X_M\}$, $\theta_2 = \{X_1, X_3, \ldots, X_M\}$, $\theta_M = \{X_1, X_2, \ldots, X_{M-1}\}$, and so forth. From these "drop-one" sets we then calculate a series of spectrograms $S^{\theta_1}(n, f)$, $S^{\theta_2}(n, f)$, ..., $S^{\theta_M}(n, f)$, each calculated from a different subset of the original data trials. $S(n, f)$ is the value of the spectrogram at the time point, n in the frequency band centered on f (see supplement 1). The jackknife estimate of the standard error of a random variable also requires that the variable be normally distributed. If we consider the spectrogram as our random variable then we must transform its values so that they form a normally distributed ensemble. One way to do this is to take the log transform of the drop-one spectrograms (Thomson and Chave 1991), with

$$S_{\text{log\_avg}}(n,f) = \ln \left[\frac{1}{M} \sum_{i=1}^{M} S^{\theta_i}(n, f) \right]$$

$$S_{\text{log\_var}}(n,f) = \frac{(M-1)}{M} \sum_{i=1}^{M} \{\ln [S^{\theta_i}(n,f)] - S_{\text{log\_avg}}\}^2 \qquad (A1)$$

Here $\ln (\cdot)$ signifies the natural log. Given $S_{\text{log\_var}}$, the 95% confidence interval at each (n, f) point in the spectrogram is $1.645 \sqrt{S_{\text{log\_var}}}(n, f) \pm S_{\text{log\_avg}}(n, f)$ (Efron and Tibshirani 1998). We restrict our consideration to the values in the $S_{\text{log\_avg}}(n, f)$ spectrogram that are in the upper quartile of a normal distribution fit to the log-transformed power spectral densities. The lower bound of this upper quartile is unique for each $S_{\text{log\_avg}}(n, f)$ spectrogram. If the lower bound falls above the lower range of the confidence interval constructed from the jackknife procedure at some point (n, f), then S_{avg} is set to zero at this point. Otherwise, the value of S_{avg} at (n, f) is retained. S_{avg} is obtained by taking $\exp(S_{\text{log\_avg}})$. This procedure ensures that when S_{avg} at (n, f) is retained, it is at least within the upper quartile of values in S_{avg} with an error rate of 5% set by the trial-to-trial variability in the spectrograms. Thresholded spectrograms are shown in Figs. 7 and 8. The lower bound of the upper quartile of the values in $S_{\text{log\_avg}}$ was used for the threshold (noise level) because the values in the upper quartile were typically further out in the tail of the empirical cumulative distribution than predicted by a normal distribution. Thus the values in the lower quartiles are thought to better represent the "noise" in the spectrograms.

APPENDIX B

Indicated in the thresholded spectrograms of Fig. 8 are the maximum values in the time and frequency domains shown by the white filled circles (or half circles as in Fig. 8, C and D). The frequency dimension ranges from 4 to 31 Hz in 70 equal steps produced by the zero padding before taking the FFT (see SUPPLEMENT 1). The time dimension ranges from 250 ms before the saccade to 250 ms after saccade onset in 10-ms steps. The maximum values are obtained by fitting a quadratic polynomial to each of 70 $S_{\text{avg}}(N, f)$ functions (each 50 time elements in length) and to each of 50 $S_{\text{avg}}(n, F)$ functions (each 70 elements in length). The search for the global maximum of each function is assisted by making adjustments in which samples around the numerical maximum are used for fitting the quadratic polynomial (Tsai and Victor 2003). These adjustments depend on the position of the numerical maximum in the function, and on the rate of change around the maximum. The number of samples used for the fits is typically small. Thus estimates of the maxima have easily interpretable significance but less certainty. However, the maxima in the

dimensions of time and frequency are extracted from multiple independent functions (for both time or frequency). This reduces the error in the estimates of the maxima.

APPENDIX C

The membership of special groups of centroids or maxima in clusters formed by a distance measurement in the time–frequency plane has to be evaluated against the null hypothesis that the partitioning could happen by chance alone. The groups are bivariate. For example, *group 1* and *group 2* can be formed based on the directions of the saccades associated with the centroids (contraversive or ipsiversive), recording location (*group 1* for occipital lobe and *group 2* for temporal lobe centroids, or *group 1* for left occipital and *group 2* for right occipital), or based on the timing of the stimulus transient (*group 1* for a presaccadic stimulus and *group 2* for a postsaccadic stimulus transition). For the counts of the members of the 2 groups in 2 time–frequency clusters,

$$a_{11}, \quad a_{12}, \quad a_{21}, \quad a_{22} \qquad (C1)$$

where a_{11} is the number of members of *group 1* in *cluster 1*, a_{12} is the number of members of *group 2* in *cluster 1*, a_{21} is the number of members of *group 1* in *cluster 2*, and a_{22} is the number of members of *group 2* in *cluster 2*.

The decrease in disorder produced by the clustering is calculated as

$$\sum_{i=1}^{2} \sum_{j=1}^{2} p(C_i, G_j) \log_2 \left[\frac{p(C_i, G_j)}{p(C_i)p(G_j)} \right] \qquad (C2)$$

Here $p(C_i, G_j) = a_{ij}/a_{total}$, with $a_{total} = a_{11} + a_{12} + a_{21} + a_{22}$.

The probability of a group member winding up in either of the 2 clusters is set to $p(C_1) = (a_{11} + a_{12})/a_{total}$, and $p(C_2) = (a_{21} + a_{22})/a_{total}$, the marginal probabilities for the clusters. The marginal probabilities for the groups must reflect the numbers from the groups in the particular subset of centroids or maxima that are being clustered. Thus $p(G_1) = (a_{11} + a_{21})/a_{total}$ and $p(G_2) = (a_{12} + a_{22})/a_{total}$. If any of the entries $a_{ij} = 0$, then the corresponding term (i, j) in the sum (*Eq. C2*) is set to zero.

Equation C2 is calculated for each branch point in a cluster tree for the groups defined by saccade direction, recording location, and stimulus timing. To determine whether the 2 clusters produced at the branch represent a clustering in time–frequency for any of the groups, the value produced by *Eq. C2* is located in a cumulative distribution function that is constructed by calculating *Eq. C2* for 1,000 sets of values a_{11}, a_{12}, a_{21}, and a_{22}. The number of members of *group 1* in *cluster 1* is used as the upper limit for the partitioning of *group 1* between 2 clusters by a binominal random number generator with the probability of success or failure for inclusion in a cluster set to 0.5. For example, if the number of centroids in a particular time–frequency cluster associated with contraversive saccades is 5, then a_{11} can be set to a value ranging from 0 to 5 (chosen by the binomial random number generator with $P = 0.5$), and a_{21} is set to $5 - a_{11}$. Similarly, if the number of ipsiversive saccades in the other cluster is 15, then a_{22} can be set to a value ranging from 0 to 15 (chosen by the binomial random number generator with $P = 0.5$), and a_{12} is set to $15 - a_{22}$.

The goal here is to determine the likelihood of the mapping of saccade direction onto 2 clusters isolated on the basis of a distance metric in the time–frequency plane. That is, how often can one get the value for *Eq. C2* that is based on measurements from a distribution of the groups in the time–frequency plane by chance alone? An empirical cumulative distribution function can be produced from the sample of values assembled by calculating *Eq. C2* 1,000 times with input variables obtained from running the binomial random number generator 1,000 times to produce both the a_{11} (and a_{21}) values and the a_{22} (and a_{12}) values. The value of *Eq. C2* that is >95% of all the simulated values can be read off from this empirical cumulative probability distribution. If the value of *Eq. C2* produced from the clustering of the centroids is equal to or greater than this 95% value, then the partitioning of the groups into the time–frequency clusters is held to be significant.

REFERENCES

Adams MM, Hof PR, Gattass R, Webster MJ, and Ungerleider LG. Visual cortical projections and chemoarchitecture of macaque monkey pulvinar. *J Comp Neurol* 419: 377–393, 2000.

Andersen RA. Multimodal integration for the representation of space in the posterior parietal cortex. *Philos Trans R Soc Lond B Sci* 352: 1421–1428, 1997.

Andersen RA, Snyder LH, Li CS, and Stricanne B. Coordinate transformations in the representation of spatial information. *Curr Opin Neurobiol* 3: 171–176, 1993.

Barash S, Bracewell RM, Fogassi L, Gnadt JW, and Andersen RA. Saccade-related activity in the lateral intraparietal area. I. Temporal properties; comparison with area 7a. *J Neurophysiol* 66: 1095–1108, 1991a.

Barash S, Bracewell RM, Fogassi L, Gnadt JW, and Andersen RA. Saccade-related activity in the lateral intraparietal area. II. Spatial properties. *J Neurophysiol* 66: 1109–1124, 1991b.

Barlow JS. Brain information processing during reading: electrophysiological correlates. *Dis Nerv Syst* 32: 668–672, 1971.

Bender DB. Retinotopic organization of macaque pulvinar. *J Neurophysiol* 46: 672–692, 1981.

Benevento LA and Rezak M. The cortical projections of the inferior pulvinar and adjacent lateral pulvinar in the rhesus monkey (*Macaca mulatta*): an autoradiographic study. *Brain Res* 108: 1–24, 1976.

Brooks DC and Gershon MD. Eye movement potentials in the oculomotor and visual systems of the cat: a comparison of reserpine induced waves with those present during wakefulness and rapid eye movement sleep. *Brain Res* 27: 223–239, 1971.

Bruce CJ. Integration of sensory and motor signals in primate frontal eye fields. In: *Signal and Sense: Local and Global Order in Perceptual Maps*, edited by Edelman GM, Gall WE, and Cowan WM. New York: Wiley-Liss, 1990, p. 261–314.

Bruce CJ and Goldberg ME. Primate frontal eye fields. I. Single neurons discharging before saccades. *J Neurophysiol* 53: 606–635, 1985.

Bruce CJ, Goldberg ME, Bushnell MC, and Stanton GB. Primate frontal eye fields. II. Physiological and anatomical correlates of electrically evoked eye movements. *J Neurophysiol* 54: 714–734, 1985.

Burkhalter AH. Cortical circuits for bottom-up and top-down processing. *Soc Neurosci Abstr* 28: 3.2, 2002.

Cai RH, Pouget A, Schlag-Rey M, and Schlag J. Perceived geometrical relationships affected by eye-movement signals. *Nature* 386: 601–604, 1997.

Carandini M, Heeger DJ, and Senn W. A synaptic explanation of suppression in visual cortex. *J Neurosci* 22: 10053–10065, 2002.

Chandra R and Optican LM. Detection, classification, and superposition resolution of action potentials in multiunit single-channel recordings by an on-line real-time neural network. *IEEE Trans Biomed Eng* 44: 403–412, 1997.

Colby CL, Duhamel JR, and Goldberg ME. Oculocentric spatial representation in parietal cortex. *Cereb Cortex* 5: 470–481, 1995.

Corbetta M and Shulman GL. Control of goal-directed and stimulus-driven attention in the brain. *Nat Rev Neurosci* 3: 201–215, 2002.

DiCarlo JL and Maunsell JHR. Form representation in monkey inferotemporal cortex is virtually unaltered by free viewing. *Nat Neurosci* 3: 814–821, 2000.

Duhamel J-R, Colby CL, and Goldberg ME. The updating of the representation of visual space in parietal cortex by intended eye movements. *Science* 255: 90–92, 1992.

Efron B and Tibshirani R. *An Introduction to the Bootstrap* (2nd ed.). Boca Raton, FL: CRC LLC, 1998.

Evans CC. Spontaneous excitation of the visual cortex and association areas—lambda waves. *Electroencephalogr Clin Neurophysiol* 5: 69–74, 1953.

Feldman M and Cohen B. Electrical activity in the lateral geniculate body of the alert monkey associated with eye movements. *J Neurophysiol* 31: 455–466, 1968.

Fourment A, Calvet J, and Bancaud J. Electrocorticography of waves associated with eye movements in man during wakefulness. *Electroencephalogr Clin Neurophysiol* 40: 457–469, 1976.

Freeman TCB, Durand S, Kiper DC, and Carandini M. Suppression without inhibition in visual cortex. *Neuron* 35: 759–771, 2002.

Funahashi S, Bruce CJ, and Goldman-Rakic PS. Mnemonic coding of visual space in the monkey's dorsolateral prefrontal cortex. *J Neurophysiol* 61: 331–349, 1989.

Gallant JL, Conner CE, and Van Essen DC. Neural activity in areas V1, V2 and V4 during free viewing of natural scenes compared to controlled viewing. *Neuroreport* 9: 2153–2158, 1998.

Gattass R, Sousa APB, and Gross CG. Visuotopic organization and extent of V3 and V4 of the macaque. *J Neurosci* 8: 1831–1845, 1988.

Gawne TJ and Woods JM. The responses of visual cortical neurons encode differences across saccades. *Neuroreport* 14: 105–109, 2003.

Gnadt JW and Andersen RA. Memory related motor planning activity in posterior parietal cortex of macaque. *Exp Brain Res* 70: 216–220, 1988.

Gottlieb J. Parietal mechanisms of target representation. *Curr Opin Neurbiol* 12: 134–140, 2002.

Gottlieb J, Kusunoki M, and Goldberg ME. The representation of visual salience in monkey parietal cortex. *Nature* 391: 481–484, 1998.

Green J. Some observations on lambda waves and peripheral stimulation. *Electroencephalogr Clin Neurophysiol* 9: 591–704, 1957.

Grenier F, Timofeev I, and Steriade M. Leading role of thalamic over cortical neurons during postinhibitory rebound excitation. *Proc Natl Acad Sci USA* 95: 13929–13934, 1998.

Gutierrez C and Cusick CG. Area V1 in macaque monkeys projects to multiple histochemically defined subdivisions of the inferior pulvinar complex. *Brain Res* 765: 349–356, 1997.

Gutkin BS, Laing CR, Colby CL, Chow CC, and Ermentrout GB. Turning on and off with excitation: the role of spike-timing asynchrony and synchrony in sustained neural activity. *J Comput Neurosci* 11: 121–134, 2001.

Hu B, Steriade M, and Deschenes M. The cellular mechanism of thalamic ponto-geniculo-occipital waves. *Neuroscience* 31: 25–35, 1989.

Jarvis MR and Mitra PP. Sampling properties of the spectrum and coherency of sequences of action potentials. *Neural Comput* 13: 717–749, 2001.

Jeannerod M and Sakai K. Occipital and geniculate potentials related to eye movements in the unanaesthetized cat. *Brain Res* 19: 361–377, 1970.

Judge SJ, Wurtz RH, and Richmond BJ. Vision during saccadic eye movements. I. Visual interactions in striate cortex. *J Neurophysiol* 43: 1133–1155, 1980.

Kalik SF, Schiff ND, Reich DS, and Purpura KP. Saccade generation during free viewing in a pattern recognition paradigm. *Soc Neurosci Abstr* 25: 147.1, 1999.

Klostermann W, Kömpf D, Heide W, Verleger R, Wauschkuhn B, and Seyfert T. The presaccadic cortical negativity prior to self-paced saccades with and without visual guidance. *Electroencephalogr Clin Neurophysiol* 91: 219–228, 1994.

Krekelberg B, Kubischik M, Hoffmann K-P, and Bremmer F. Neural correlates of visual localization and perisaccadic mislocalization. *Neuron* 37: 537–545, 2003.

Lee D and Malpeli JG. Effects of saccades on the activity of neurons in the cat lateral geniculate nucleus. *J Neurophysiol* 79: 922–936, 1998.

Leichnetz GR and Goldberg ME. Higher centers concerned with eye movement and visual attention: cerebral cortex and thalamus. In: *Neuroanatomy of the Oculomotor System*, edited by Büttner-Ennever JA. Amsterdam: Elsevier, 1988, p. 365–429.

Martin RF and Bowden DM. *Primate Brain Maps: Structure of the Macaque Brain*. New York: Elsevier Science, 2000.

McCloskey DI. Corollary discharges: motor command and perception. In *Handbook of Physiology. The Nervous System*. Bethesda, MD: Am. Physiol. Soc., 1981, sect. 1, vol. II, chapt. 32, p. 1415–1447.

Mitra PP and Pesaran B. Analysis of dynamic brain imaging data. *Biophys J* 76: 691–708, 1999.

Morrone MC, Ross J, and Burr DC. Apparent position of visual targets during real and simulated saccadic eye movements. *J Neurosci* 17: 7941–7953, 1997.

Niemeier M, Crawford JD, and Tweed DB. Optimal transsaccadic integration explains distorted spatial perception. *Nature* 422: 76–80, 2003.

Ölveczky BP, Baccus SA, and Meister M. Segregation of object and background motion in the retina. *Nature* 423: 401–408, 2003.

Percival DB and Walden AT. *Spectral Analysis for Physical Applications*. Cambridge, UK: Cambridge Univ. Press, 1993.

Pesaran B, Pezaris JS, Sahani M, Mitra PP, and Andersen RA. Temporal structure in neuronal activity during working memory in macaque parietal cortex. *Nat Neurosci* 5: 805–811, 2002.

Purpura KP, Kalik SF, and Schiff ND. Cues for object surface orientation drive neural responses in inferotemporal cortex. *Soc Neurosci Abstr* 25: 370.6, 1999.

Ramcharan EJ, Gnadt JW, and Sherman SM. The effects of saccadic eye movements on the activity of geniculate relay neurons in the monkey. *Vis Neurosci* 18: 253–258, 2001.

Reppas JB, Usrey WM, and Reid RC. Saccadic eye movements modulated visual responses in the lateral geniculate nucleus. *Neuron* 35: 961–974, 2002.

Richmond BJ, Hertz JA, and Gawne TJ. The relation between V1 neuronal responses and eye movement-like stimulus presentations. *Neurocomputing* 26/27: 247–254, 1999.

Robinson DL, Petersen SE, and Keys W. Saccade-related and visual activities in the pulvinar nuclei of the behaving rhesus monkey. *Exp Brain Res* 62: 625–634, 1986.

Roska B and Werblin F. Rapid global shifts in natural scenes block spiking in specific ganglion cell types. *Nat Neurosci* 6: 600–608, 2003.

Ross J, Morrone MC, Goldberg ME, and Burr DC. Changes in visual perception at the time of saccades. *Trends Neurosci* 24: 113–121, 2001.

Schall JD. Neuronal activity related to visually guided saccadic eye movements in the supplementary motor area of rhesus monkeys. *J Neurophysiol* 66: 530–558, 1991.

Schall JD and Hanes DP. Neural basis of saccade target selection in frontal eye field during visual search. *Nature* 366: 467–469, 1993.

Schall JD and Thompson KG. Neural selection and control of visually guided eye movements. *Annu Rev Neurosci* 22: 241–259, 1999.

Schlag J and Schlag-Rey M. Visuomotor functions of central thalamus in monkey. II. Unit activity related to visual events, targeting, and fixation. *J Neurophysiol* 51: 1175–1195, 1984.

Schlag-Rey M and Schlag J. Visuomotor functions of central thalamus in monkey. I. Unit activity related to spontaneous eye movements. *J Neurophysiol* 51: 1149–1174, 1984.

Seidemann E, Arieli A, Grinvald A, and Slovin H. Dynamics of depolarization and hyperpolarization in the frontal cortex and saccade goal. *Science* 295: 862–865, 2002.

Shao Z and Burkhalter A. Role of GABA$_B$ receptor-mediated inhibition in reciprocal interareal pathways of rat visual cortex. *J Neurophysiol* 81: 1014–1024, 1999.

Shipp S. Corticopulvinar connections of areas V5, V4, and V3 in the macaque monkey: a dual model of retinal and cortical topographies. *J Comp Neurol* 439: 469–490, 2001.

Skrandies W and Laschke K. Topography of visually evoked brain activity during eye movements: lambda waves, saccadic suppression, and discrimination performance. *Int J Psychophysiol* 27: 15–27, 1997.

Snodderly DM and Gur M. Organization of striate cortex (V1) of alert, trained monkeys (*Macaca fascicularis*): ongoing activity, stimulus selectivity, and widths of receptive field activating regions. *J Neurophysiol* 74: 2100–2125, 1995.

Sobotka S, Nowicka A, and Ringo JL. Activity linked to externally cued saccades in single units recorded from hippocampal, parahippocampal, and inferotemporal areas of macaques. *J Neurophysiol* 78: 2156–2163, 1997.

Sobotka S and Ringo JL. Saccadic eye movements, even in darkness, generate event-related potentials recorded in medial septum and medial temporal cortex. *Brain Res* 756: 168–173, 1997.

Sobotka S, Zuo W, and Ringo JL. Is the functional connectivity within temporal lobe influenced by saccadic eye movements? *J Neurophysiol* 88: 1675–1684, 2002.

3478   K. P. PURPURA, S. F. KALIK, AND N. D. SCHIFF

Sommer MA and Wurtz RH. A pathway in primate brain for internal monitoring of movements. *Science* 296: 1480–1482, 2002.

Sutter EE. A deterministic approach to nonlinear systems analysis. In: *Nonlinear Vision: Determination of Neural Receptive Fields, Function, and Networks*, edited by Pinter RB and Nabet B. Boca Raton, FL: CRC, 1992, p. 171–220.

Swadlow HA, Gusev AG, and Bezdudnaya T. Activation of a cortical column by a thalamocortical impulse. *J Neurosci* 22: 7766–7773, 2002.

Thiele A, Henning P, Kubischik M, and Hoffmann K-P. Neural mechanisms of saccadic suppression. *Science* 295: 2460–2462, 2002.

Thomson DJ. Spectrum estimation and harmonic analysis. *Proc IEEE* 70: 1055–1096, 1982.

Thomson DJ. Multiple window method for obtaining improved spectrograms of signals. U.S. Patent US 6,351,729 B1, 2002.

Thomson DJ and Chave AD. Jackknifed error estimates for spectra, coherences, and transfer functions. In *Advances in Spectrum Analysis and Array Processing*, edited by Haykin S. Englewood Cliffs, NJ: Prentice-Hall, 1991, p. 58–113.

Tsai JJ and Victor JD. Reading a population code: a multi-scale neural model for representing binocular disparity. *Vision Res* 43: 445–466, 2003.

Umeno MM and Goldberg ME. Spatial processing in the monkey frontal eye field. I. Predictive visual responses. *J Neurophysiol* 78: 1373–1383, 1997.

Ungerleider LG, Galkin TW, and Mishkin M. Visuotopic organization of projections from striate cortex to inferior and lateral pulvinar in rhesus monkey. *J Comp Neurol* 217: 137–157, 1983.

Wallenstein GV, Eichenbaum H, and Hasselmo ME. The hippocampus as an associator of discontiguous events. *Trends Neurosci* 21: 317–323, 1998.

Webster MJ, Bachevalier J, and Ungerleider LG. Connections of inferior temporal areas TEO and TE with parietal and frontal cortex in macaque monkeys. *Cereb Cortex* 4: 470–483, 1994.

Wurtz RH. Vision for the control of movement. *Invest Ophthalmol Vis Sci* 37: 2131–2145, 1996.

Yarrow K, Haggard P, Heal R, Brown P, and Rothwell JC. Illusory perceptions of space and time preserve cross-saccadic perceptual continuity. *Nature* 414: 302–305, 2001.